Atmospheric Research 309 (2024) 107568

Contents lists available at ScienceDirect

Atmospheric Research

journal homepage: www.elsevier.com/locate/atmosres

Near-surface wind speed trends and variability over the Antarctic Peninsula, 1979–2022

Miguel Andres-Martin [a,b,*], Cesar Azorin-Molina [a], Encarna Serrano [b], Sergi González-Herrero [c,d], Jose A. Guijarro [e], Shalenys Bedoya-Valestt [a], Eduardo Utrabo-Carazo [a], Sergio M. Vicente Serrano [f]

[a] Centro de Investigaciones sobre Desertificación, Consejo Superior de Investigaciones Científicas (CIDE, CSIC-UV-Generalitat Valenciana), Climate, Atmosphere and Ocean Laboratory (Climatoc-Lab), Moncada, Valencia, Spain
[b] Facultad CC. Físicas, Universidad Complutense de Madrid, Madrid, Spain
[c] Antarctic Group, State Meteorological Agency (AEMET), Barcelona, Spain
[d] WSL Institute for Snow and Avalanche Research SLF, Davos, Switzerland
[e] Retired from the State Meteorological Agency (AEMET), Balearic Islands Office, Palma de Mallorca, Spain
[f] Instituto Pirenaico de Ecología, Consejo Superior de Investigaciones Científicas (IPE–CSIC), Zaragoza, Spain

ARTICLE INFO

Keywords:
Antarctic Peninsula
Surface wind speed trends
Southern Annular Mode
Southern Oscillation Index
ERA5
Wind speed observations

ABSTRACT

Near-Surface Wind Speed (SWS) is a crucial but less studied climate variable in the northern Antarctic Peninsula (AP). This research evaluates, for the first time, 44 years (i.e., 1979–2022) of SWS trends and variability across the AP using two data sources: (i) observational data from quality-controlled and homogenized meteorological stations, and (ii) reanalysis data from ERA5; the accuracy of this product strongly depends on each station with an overall underestimation of observed SWS. Annual trends in observed SWS exhibit a positive trend, being statistically significant in autumn and spring, with a marked intraanual and spatial variability in the sign and magnitudes across the AP. In addition, the multidecadal variability of observed SWS showed a general positive trend until ~2001 (varying between 1993 and 2007 depending on each season), followed by a period of slowdown in the last two decades. Over the AP, SWS changes are mainly driven by two principal modes of atmospheric variability: i.e., mainly the Southern Annular Mode (SAM) and, secondarily, by the El Niño-Southern Oscillation (ENSO). Overall, positive trends in SWS could be partly associated with the increase and poleward shift of the westerlies due to the positive trend of the SAM index. However, as previous studies pointed out for air temperature and precipitation, we found a non-stationary and complex relationship of these modes with SWS changes. This research addresses the gap in SWS changes and variability in the AP and surrounding Southern Ocean and the influence of the atmospheric circulation, a hotspot area in climate change research.

1. Introduction

Near-surface wind speed (SWS) has been the forgotten part of climate change research compared to studies dealing with e.g., air temperature or precipitation (Zeng et al., 2019), mainly due to the lower availability of observed wind data and the existing problems with the instruments (Azorin-Molina et al., 2014; IPCC, 2021; Utrabo-Carazo et al., 2022). During the last two decades, thanks to the increased interest in SWS changes and variability, two processes have been identified using observations over different regions of the globe: the first one, termed "stilling" (Roderick et al., 2007), consists in a decrease of SWS until ~2010 (Azorin-Molina et al., 2014, 2016, 2018a; McVicar et al., 2012; Minola et al., 2016; G. Zhang et al., 2020) followed by the second, named "*reversal*", implying a cessation of the "*stilling*" and a recovery of SWS (Minola et al., 2021; Utrabo-Carazo et al., 2022; Zeng et al., 2019; Zhang and Wang, 2020).

Although some studies have dealt with strong wind speed events (Yu and Zhong, 2019a) or wind energy applications (Yu et al., 2020), there is a dearth of research focused on SWS changes and variability in the Antarctic climate (Yu and Zhong, 2019a, 2019b). Marshall (2002)

* Corresponding author at: Centro de Investigaciones sobre Desertificación, Consejo Superior de Investigaciones Científicas (CIDE-CSIC-UV-GVA), Ctra. CV-315 km 10.7, 46113 Moncada, Valencia, Spain.
E-mail address: miguel.andres@csic.es (M. Andres-Martin).

https://doi.org/10.1016/j.atmosres.2024.107568
Received 21 March 2024; Received in revised form 18 June 2024; Accepted 30 June 2024
Available online 1 July 2024

investigated wind speed trends at 500 hPa and 850 hPa levels based on radiosonde observations from Bellingshausen station, as well as NCEP–NCAR and ERA-15 data; statistically significant positive trends were identified in the zonal (u) annual average. Turner et al. (2005) analyzed SWS trends at Antarctic stations using data from the SCAR MET-READER database up to 2000, reporting a positive trend in SWS at Rothera, Bellingshausen, and Faraday/Vernadsky ($p < 0.05$ during summer). More recently, Van Wessem et al. (2015) compared SWS trends between the Regional Atmospheric Climate Model (RACMO) 2.3 forced with ERA-Interim and SCAR MET-READER stations for the period 1979–2013, revealing a contrasting gradient in SWS trends between the western (positive trends) and eastern (negative trends) coasts of the Antarctic Peninsula (AP).

The Southern Annular Mode (SAM) is the main mode of variability controlling the extratropical Southern Hemisphere climate, playing a pivotal role in temperature, precipitation or wind speed (Clem and Fogt, 2013; Clem et al., 2016; Carrasco et al., 2021; Fogt and Marshall, 2020). SAM is associated with changes in the position and strength of the southern westerly winds (Fogt and Marshall, 2020). Over the last decades, there has been a change in the atmospheric circulation over the AP: a poleward shift of the circumpolar westerly belt (Deng et al., 2022; Thompson and Solomon, 2002) attributed to a positive trend of SAM. The SAM index has displayed a general positive trend since 1958, mainly related to stratospheric ozone depletion and greenhouse gasses increase (Thompson and Solomon, 2002), and it is projected to continue increasing over the 21st century (Deng et al., 2022). El Niño-Southern Oscillation (ENSO) plays a secondary role in the climate variability of AP compared with SAM. In particular, it is usually coupled with SAM and also affects the depth and extension of the Amundsen Sea Low (ASL) (Clem et al., 2016; Clem and Fogt, 2013). Positive SAM increases the zonal wind and intensifies the ASL (Hosking et al., 2013). The cold (warm) phase of the ENSO is associated with a deepening (filling) of the ASL (Raphael et al., 2016). When El Niño (La Niña) events occur under positive (negative) SAM, ENSO and SAM are in phase and the influence of ENSO is remarkable (Clem and Fogt, 2013). There two modes of variability are key in order to understand SWS changes and its implication on the AP.

SWS has direct impacts on the AP climate. Over the second half of the 20th century, the AP has experienced significant warming (Jones et al., 2019; Marshall, 2007). The increased warming over the northeastern side of the AP is wind-driven, linked to the advection of warm maritime air by the increase in westerlies over the AP (Marshall, 2002). Consequently, strong winds cross the AP mountain barrier, enhancing the occurrence of the well-known “Foehn phenomenon” (Orr et al., 2008), and producing a large impact on the surface melt in the Larsen C ice shelf (Cape et al., 2015; Elvidge et al., 2020; Laffin et al., 2023). This effect caused the air temperature records settled in recent years (Bozkurt et al., 2018; González-Herrero et al., 2022; Xu et al., 2021). SWS and its variability has also been connected with multiple climate impacts, causing a modest decrease in sea ice extent (Holland et al., 2017), an enhanced zonal geostrophic flow of the Antarctic Circumpolar Current (Liau and Chao, 2017), an increase in the precipitation on the western side of the AP (Marshall et al., 2017), controlling Antarctic Bottom Water formation (Schmidt et al., 2023), among others.

The Antarctic region has become a hotspot in climate change research because of its sensitivity to global warming (González-Herrero et al., 2024). In view of: (i) the crucial roles of SWS in the AP climate and (ii) the research gap in assessing changes and multidecadal variability of SWS and its potential causes over this region, this study aims to quantify SWS multidecadal variability and trends over the northern AP. Here we also explore its likely dynamic mechanisms, in particular the control exerted by the leading coupled modes of oceanic-atmospheric variability (SAM and El Niño-Southern Oscillation -ENSO-). Up to our knowledge, this is the longest assessment investigating SWS trends and variability and its likely causes over the AP, covering the 44-year 1979–2022 period.

2. Data and methods

2.1. Study area

The AP is the northernmost tip of Antarctica and it extends from the base of the continent at ~73°S until ~63°S (Fig. 1a). It consists of a mountain range with highest elevations between 800 m above sea level (m a.s.l.) in the northern fringe to 2000 m a.s.l. in the central-southern parts. Along with its complex topography, two pressure systems, on each side of the AP, impact the climate (Fig. S1) (Clem et al., 2016; Oliva et al., 2017).

In the western AP, the ASL (Raphael et al., 2016) transports relatively warm and moist air masses from the northwest. The mountain ridge acts as a barrier to Southern Hemisphere westerly winds, creating a foehn effect that brings warm and dry air to the eastern side (Orr et al., 2008). However, the Weddell Sea Low prevails over the eastern side, bringing cold and dry air masses from southerly barrier winds, creating a polar continental climate (Carrasco et al., 2021). Consequently, due to the influence of these pressure systems and the topography, the western side of the AP is warmer and wetter, while the eastern side is colder and dryer (Oliva et al., 2017).

2.2. Observational data

Two different observational datasets were used. First, we analyzed monthly averages from the SWS data provided by the SCAR MET-READER project (Turner et al., 2004). The series are publicly available at https://legacy.bas.ac.uk/met/READER/data.html (last accessed February 28, 2024) covering the 1979–2022 period. Specifically, we used the data of seven stations (for locations see Fig. 1a; details are given in Table S1) covering different parts of the northern AP and at least operating since 1979. Although different levels of reliability appear in the SCAR MET-READER data depending on the source and the number of observations available to calculate the monthly means, we downloaded all the available time series for those 7 stations. Detailed information about data quality is given inhttps://legacy.bas.ac.uk/met/READER/data.html (last accessed May 20, 2024), and the SCAR MET-READER project and stations were described by Turner et al. (2004). In addition, we evaluated for the first time SWS series from the Spanish Base Juan Carlos I (hereafter JCI) spanning the 34 years from 1988 to 2022. Since long-term observations are lacking in the AP due to the harsh environmental conditions (Wang et al., 2021), the data from the JCI is highly valuable, as it adds unexplored SWS observations to the SCAR MET-READER network in the AP. This station is located on the South Shetland Islands, specifically on Livingston Island, and has been collecting SWS data since February 1988. The geographic position of JCI is remarkable, located at 50 m of South Bay, with the 275 m a.s.l. barrier of the Mount Reina Sofia to the east behind the station (see Fig. 1b). Notice that in a mountainous terrain like the AP, observational wind might be influenced by the local orography and subject to topographic blockings and accelerations. In addition, as JCI has a different timespan than the SCAR-METREADER database, we just show its results without any comparison with other stations.

2.3. Quality control and homogenization

Operational issues and limited observational data make it difficult to obtain robust and complete long-term SWS time series across the AP. To solve this constraint, a quality control and homogenization protocol has been performed by applying the R package *Climatol* (available at https://CRAN.R-project.org/package=climatol; last accessed February 28, 2024). Here we applied the same protocol used successfully in other studies around the world (i.e., Azorin-Molina et al., 2016; Minola et al., 2021; Utrabo-Carazo et al., 2022), and for the JCI data (Gonzalez et al., 2018). Although the series of the SCAR MET-READER database have gone through their own quality control, the SCAR MET-READER project

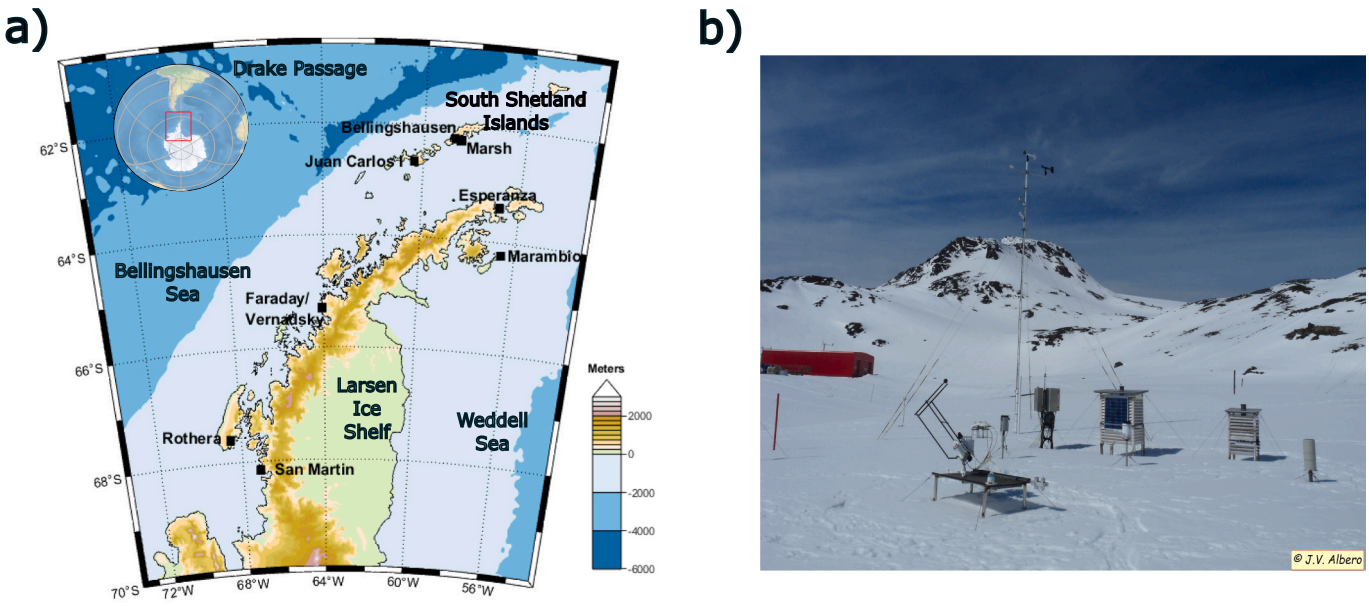

Fig. 1. (a) Location of observational stations (black filled squares) and domain used in this study (latitude: 60.5°S to 70°S; longitude: 53°W to 73°W, stations are detailed in Table S1), (b) Spanish Juan Carlos I base station located over the Livingston Island, with the Mount Reina Sofia behind (https://antartida.aemet.es/tiemporeal/?pag=tiemporeal; last accessed February 28, 2024).

recommends an extra quality control process to solve plausible limitations. We also applied this homogenization protocol to the two observational datasets to detect artificial shifts (or break-points) that create biases, and to remove them. This approach allows us to compare results between the two data sources.

The first step of the *Climatol* protocol consists in the calculation of the difference between the observed SWS data and the average of their nearest stations, all in standardized form. This difference is used to apply the Standard Normal Homogeneity Test (SNHT; Alexandersson, 1986) in two different procedures: 1) on staggered time windows, to minimize the likely masking influence of multiple break-points, and 2) on the entire series. This process is repeated iteratively until no SNHT value overtakes a user-designated threshold. This threshold is selected based on the exploratory observation of the histograms of the maximum values of SNHT. As metadata are not available, a higher threshold was selected to avoid the detection of false changes in the mean, although small inhomogeneities may pass uncorrected. As observational stations for the AP are limited and distant, in the final step of the protocol all missing values were filled using the ERA5 nearest grid point as reference series. A detailed explanation of this process can be found in Guijarro (2018). This homogenization method revealed and corrected one break-point for the stations of Esperanza, Faraday/Vernadsky and Marsh, two for San Martin and Rothera, and three for Marambio.

2.4. ERA5 reanalysis data

In Antarctica, the relative remoteness and harsh environmental conditions make observations a challenging task (Tardif et al., 2022). Long-term series are scarce (Wang et al., 2021), and it is common to use reanalysis or regional models to investigate the Antarctic climate (Caton Harrison et al., 2022; González et al., 2021). Previous studies concluded that SWS anomalies and trends differ between observations and reanalysis due to the difficulty that reanalysis systems have in reproducing long-term variability (Fan et al., 2020; Ramon et al., 2019; Torralba et al., 2017; Wohland et al., 2019). Despite these limitations, ERA5 is the most accurate reanalysis for assessing SWS changes and has been extensively used in the last decades by the wind research community (e.g. Ramon et al., 2019).

There are only a few studies dealing with the skills of different reanalysis in reproducing SWS over the study region. Gossart et al. (2019), Tetzner et al. (2019), Dong et al. (2020) or Caton Harrison et al. (2022) found generally a better reproduction of SWS by ERA5 compared with other reanalysis over Antarctica and AP. However, reanalysis should be carefully considered due to their potential weaknesses in reproducing the complex orography (Jones et al., 2019), as occurs in the AP. Even using RACMO 2.3 forced with ERA-Interim at 5.5 km of horizontal resolution over the AP, the model cannot simulate the processes related to the complex orography (Van Wessem et al., 2015).

Given the abilities and limitations of ERA5 in reproducing interannual variability and monthly magnitude of the 10-m SWS over the AP, and taking into account that the development of a dynamical downscaled climate model over land and ocean (i.e. >30 years and ~ 5 km spatial resolution) exceeds the scope of this research, ERA5 has been selected to assess SWS changes at a higher spatial resolution than site-specific observational data. ERA5 has a horizontal resolution of 31 km for land and ocean, and hourly outputs. The increased resolution with respect to its predecessor, ERA-Interim, with 10 years between them, improves the representation of near-surface winds (Hersbach et al., 2020). The monthly average data used here (1979–2022; latitude: −60.5° to −70.0°; longitude: −53.0° to −73.0°) have been downloaded from https://cds.climate.copernicus.eu/#!/search?text=ERA5&type=dataset (last accessed February 28, 2024).

2.5. Atmospheric modes of variability

Two atmospheric circulation patterns are the main drivers of the atmospheric variability across the AP: the Southern Annular Mode (SAM) and the El Niño-Southern Oscillation (ENSO) (Gonzalez et al., 2018). We used the monthly station-based SAM index calculated by Marshall (2003; available online at https://legacy.bas.ac.uk/met/gjma/sam.html; last accessed February 28, 2024). This standardized index is based on the difference in normalized zonal sea level pressure between 40.8°S and 65.8°S, calculated using 12 stations. The activity of ENSO is tracked using the index of its atmospheric component, i.e., the Southern Oscillation Index (SOI), which is standardized and based on the difference of observed sea level pressure between Tahiti and Darwin

(Australia) (downloaded from https://www.ncdc.noaa.gov/teleconnections/enso/indicators/soi/; last accessed February 28, 2024).

2.6. Statistical methods

The agreement between observational and ERA5 SWS series has been computed with: (1) Spearman's correlation coefficient (r_s). This coefficient is similar to the classic Pearson coefficient, but as it is based on ranks, it is more robust and suitable when the variable is not normally distributed; (2) Root Mean Square Error (RMSE); and (3) Mean Bias (MB; calculated as ERA5 minus observational data). The statistical significance of the bias was assessed through a Wilcoxon–Mann–Whitney test (Siegel and Castellan Jr., 1988). We selected the reanalysis grid points nearest to each station, as done in Gossart et al. (2019), Tetzner et al. (2019), and Caton Harrison et al. (2022). Additionally, we computed the station regional means for both datasets from 1979 to 2022, excluding

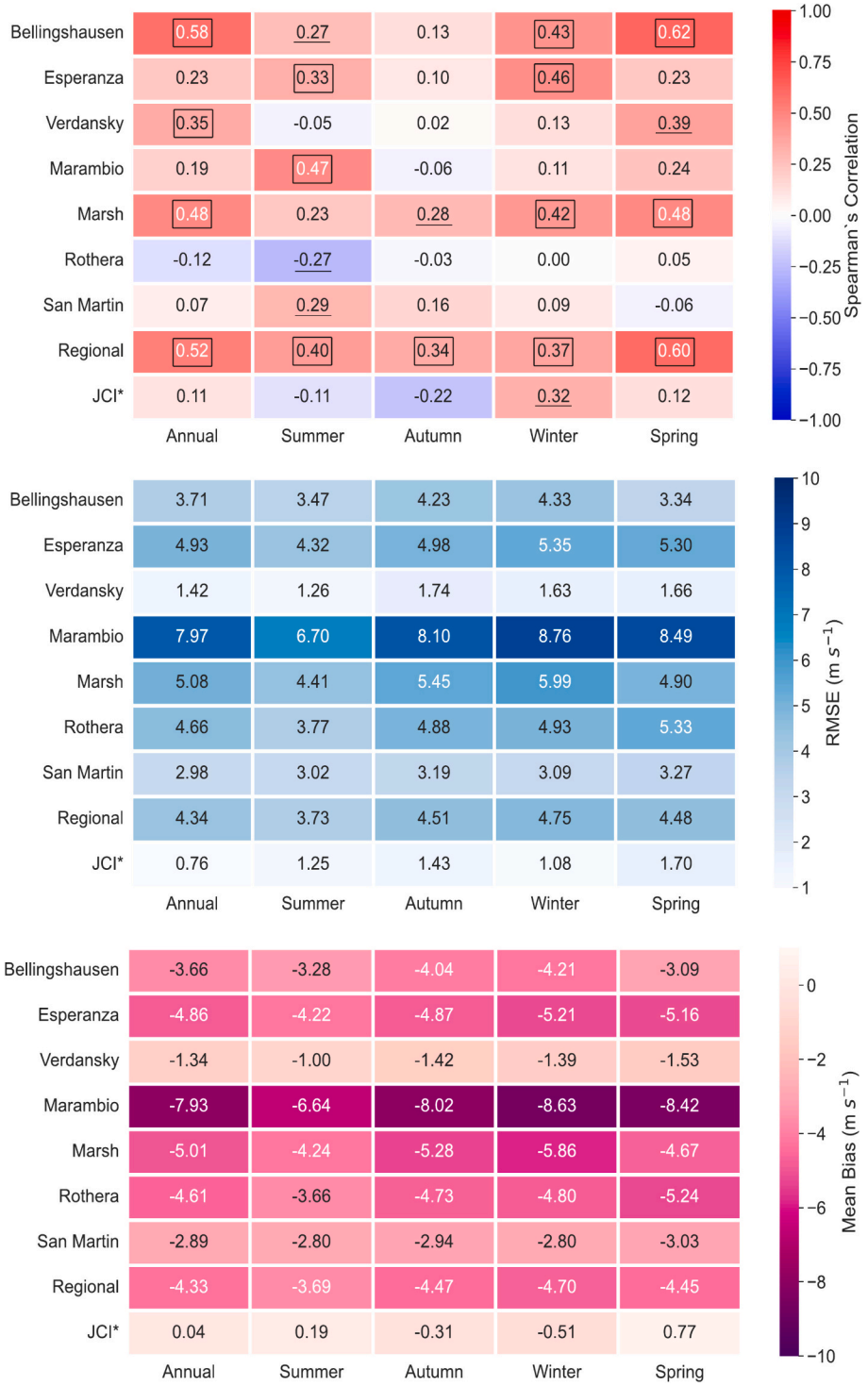

Fig. 2. Performance statistics between observational and ERA5 SWS series for 1979–2022: (a) Spearman's correlation coefficient; underlined values indicate statistical significance at $p < 0.10$, and boxed values at $p < 0.05$; (b) RMSE (m s^{-1}); and (c) MB (m s^{-1}). The asterisk in JCI indicates the different study period (1988–2022). All biases are statistically significant at $p < 0.05$.

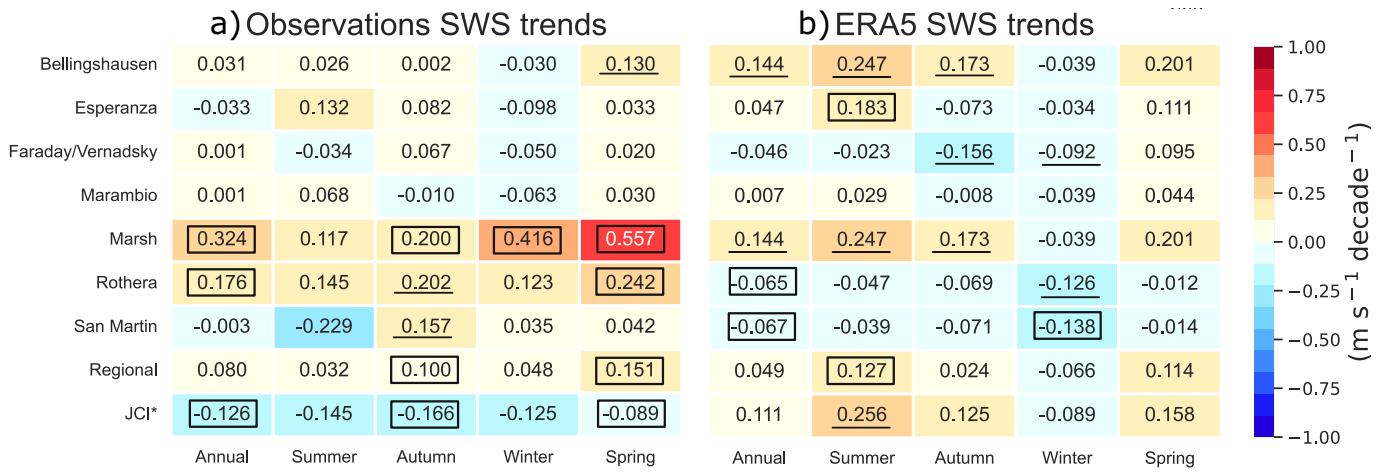

Fig. 3. Trends (in m s^{-1} dec^{-1}) of (a) SWS anomalies for observations and (b) the closest ERA5 grid points for 1979–2022. The asterisk in JCI indicates the different study period (1988–2022). Underlined values indicate statistical significance at $p < 0.10$, and boxed values at $p < 0.05$.

JCI due to its different time span.

To assess the multidecadal variability, a 10-yr Gaussian low-pass filter ($\sigma = 2.67$) has been applied to the regional mean anomalies of stations and ERA5 nearest points (computed as deviation from 1991 to 2020 period). In order to understand potential subperiods and changes in trends, we applied a piecewise linear regression model (Muggeo, 2003) to the SWS data. Given the significant interannual variability, we calculated breakpoints on the 10-year Gaussian filtered series to highlight long-term trend changes. The Score test (Muggeo, 2016) was used to assess the statistical significance of the identified turning points. The determination of SWS anomaly trends (expressed in meters per second per decade; i.e., m s^{-1} dec^{-1}) has been carried out by applying a linear regression, and its statistical significance evaluated by a non-parametric modified Mann-Kendall's tau-b test, so as to account for autocorrelation (Hamed and Rao, 1998). Moreover, to deepen the evaluation of the trends, a running trends analysis (Brunetti et al., 2006) has been computed, selecting a minimum window length of 10 years, running from 1979 to 2022 (1988 for JCI).

We performed correlation analysis and constructed anomaly composites of the atmospheric dynamics to assess the influence of variability modes on SWS. The linear relationship was evaluated using Pearson's correlation coefficient (r) between indices and SWS trends. Following Clem and Fogt (2013), we identified years with SAM/SOI values above the 70th and below the 30th percentiles for positive and negative composites, respectively. These years were selected for SWS and mean sea level pressure (MSLP) anomalies, to analyze how the different phases affect the dynamics and SWS response. A t-student test (95% confidence) was performed to determine if the SWS anomalies differ from 0.

Statistical methods have been performed using two levels of significance, distinguishing three categories: significant at $p < 0.05$, significant at $p < 0.10$, and not significant for $p > 0.10$. Calculations are performed over two different time scales: annual and seasonal. Namely, the austral seasons are: December, January and February (DJF) for summer; March, April and May (MAM) for autumn; June, July and August (JJA) for winter; and September, October and November (SON) for spring.

3. Results

3.1. Comparison between observational and ERA5 SWS

A statistical comparison between the observed SWS and ERA5 data is presented in Fig. 2, showing the results of the r_s, RMSE and MB. The station-dependence dominates the correlation, indicating that the results vary depending on the chosen station. For example, Bellingshausen presents positive r_s for all time scales, being strong and statistically significant annually (0.58, $p < 0.05$), in spring (0.62, $p < 0.05$) and winter (0.43, $p < 0.05$). Marsh and Esperanza also show a similar behavior, with positive correlations among the time scales. In addition, Rothera, San Martin and JCI show weak and generally not statistically significant results. Nevertheless, the regional mean indicates a good ERA5 performance with positive and significant correlations for all time scales. Regarding the seasonality, during autumn the r_s is weaker and less significant for all stations compared to the rest of time scales. The RMSE and MB also denote a weak seasonality, with generally lower values in summer than the rest of seasons. Furthermore, both RMSE and MB again show a more remarkable station-dependence. JCI and Faraday/Vernadsky exhibit the smallest RMSE values (< 2 m s^{-1} at JCI), whereas Marsh and, especially Marambio, present the largest ones (even >8 m s^{-1} at the latter). Regarding MB, negative values appear for most stations and time scales, with the strongest ones observed at Marambio (up to −8.63 m s^{-1}). JCI stands out as the exception, with positive MB but close to zero during spring and summer. These negative values in MB indicate that ERA5 generally underestimates observed SWS, as can be seen in Fig. S3.

3.2. Annual and seasonal wind speed trends

Fig. 3 shows the annual and seasonal SWS trends for 1979–2022 (1988–2022 for JCI). The observational regional mean shows positive trends, which are remarkable and statistically significant for autumn and spring ($p < 0.05$). As is the previous section, the station-dependence dominates the observational trends: Rothera, and particularly Marsh denote positive and generally statistically significant trends, up to +0.416 m s^{-1} dec^{-1} ($p < 0.05$) in winter and + 0.557 m s^{-1} dec^{-1} ($p < 0.05$) in spring over Marsh; JCI shows negative and generally significant trends (−0.126 and − 0.166 m s^{-1} dec^{-1} ($p < 0.05$) annually and in autumn, respectively); the rest of the stations show weak and mostly no significant results.

The comparison between the SWS trends reported in the ERA5 regional mean and in the station regional mean reveals consistent agreement in the positive trends across all time scales, except for winter where ERA5 indicates a negative trend. Additionally, certain observatories reveal discrepancies; for instance, negative trends are observed in ERA5's Rothera closest grid point (minimum of −0.126 m s^{-1} dec^{-1} ($p < 0.10$) in winter), contrasting with the positive trends observed in the stational series (+0.123 m s^{-1} dec^{-1} ($p > 0.05$) in winter). Similarly, a dominance of positive trends (except for winter) is found in JCI ERA5, whereas negative trends are detected in the observations.

Fig. 4 provides the annual and seasonal multidecadal variability of

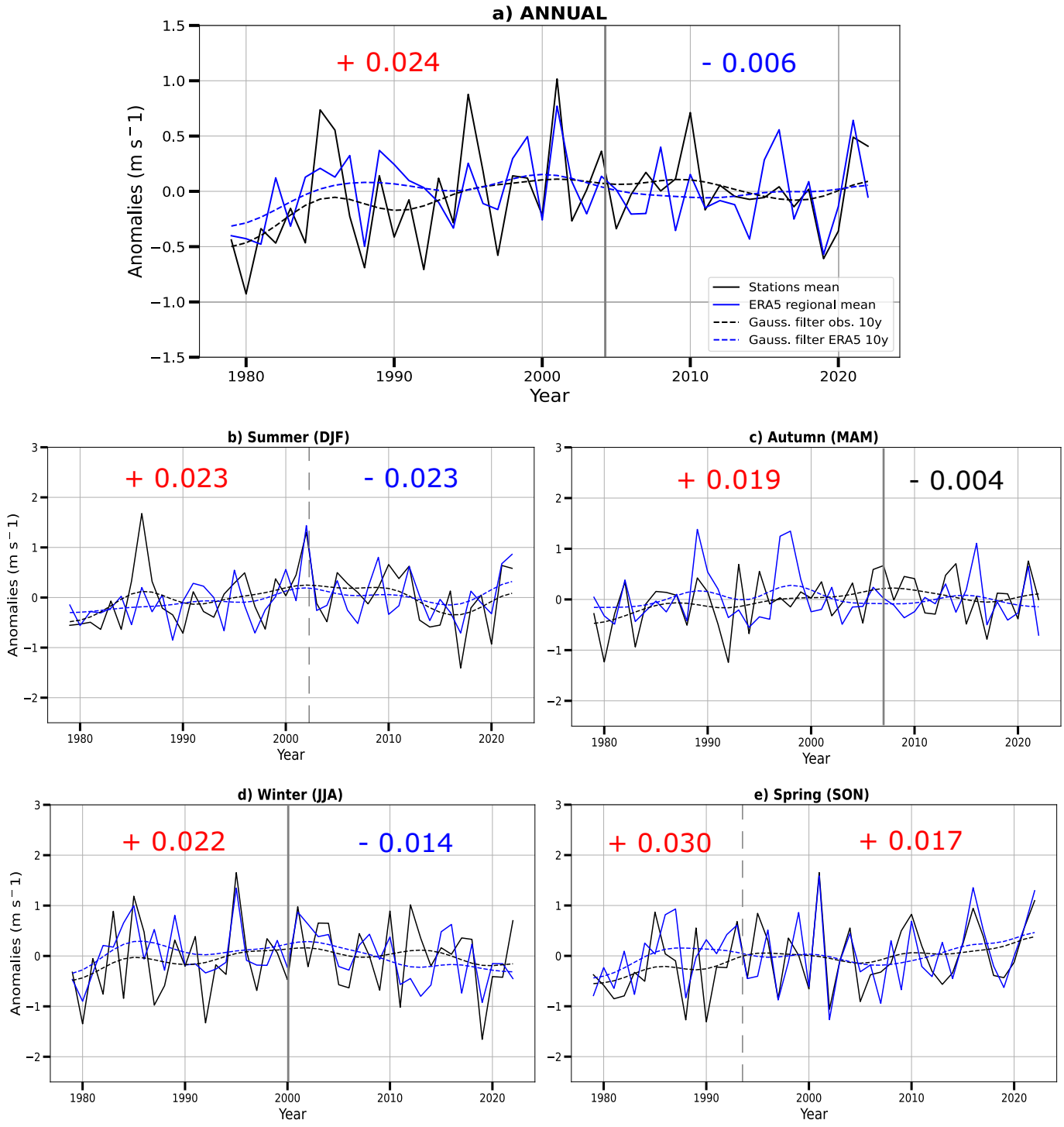

Fig. 4. Annual and seasonal regional mean (without JCI due to the different timespan) wind speed anomalies (in m s^{-1}) for observed (black line) and ERA5 (blue line). The 10-yr Gaussian low-pass filters for both datasets are shown in dashed lines. A vertical solid and dash line shows the breakpoint year ($p < 0.05$ and $p < 0.10$ respectively). The SWS anomaly trends' values (in m s^{-1} dec^{-1}) before and after the breakpoint are displayed, with colors if statistically significant ($p < 0.05$). Notice that the Y-axes range differs between the annual and seasonal plots. (For interpretation of the references to colour in this figure legend, the reader is referred to the web version of this article.)

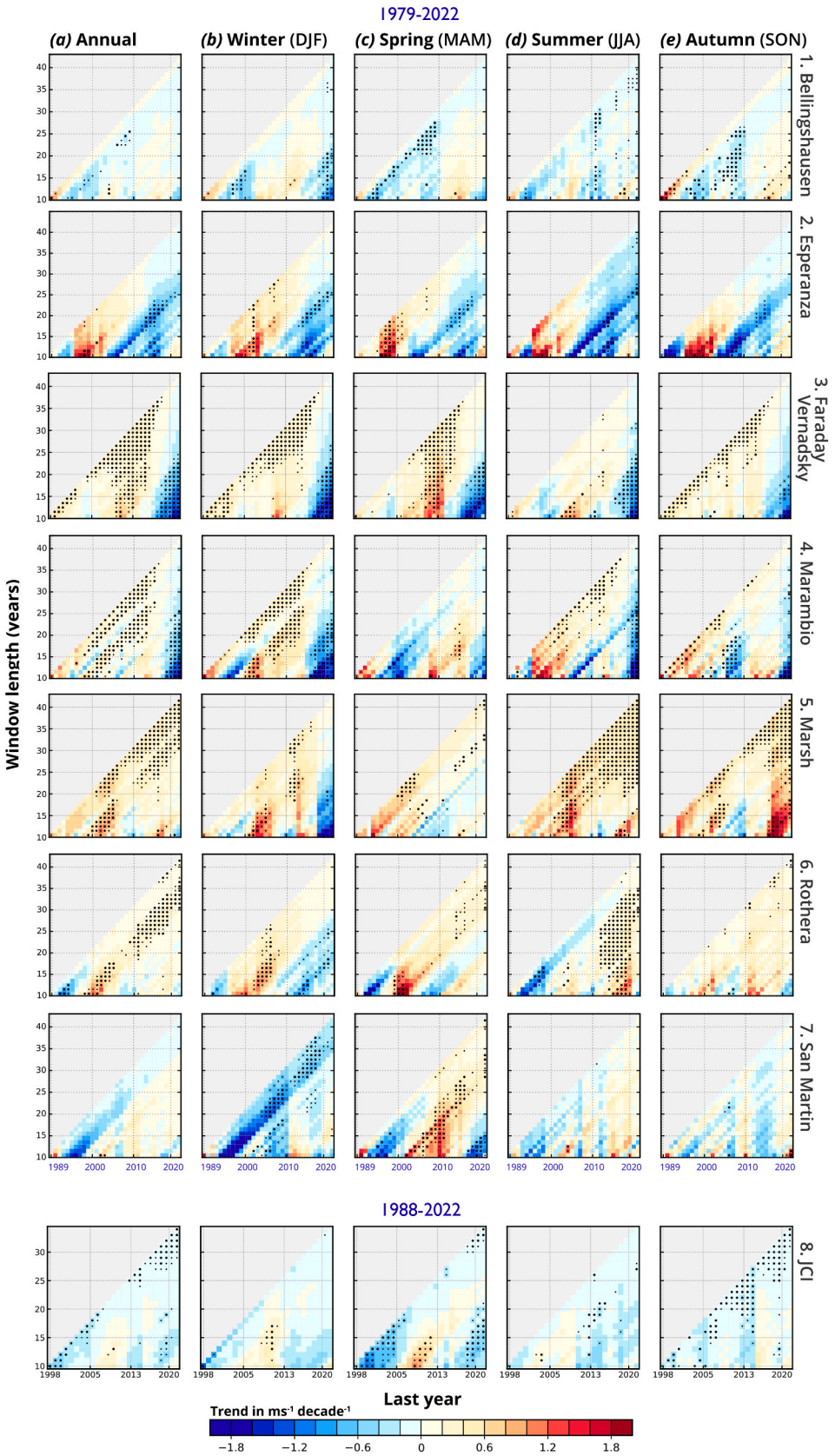

Fig. 5. Running trend analysis of SWS anomalies (in m s^{-1} dec^{-1}) for all observational data. Small black dots represent significance at $p < 0.10$ and the big dot at $p < 0.05$. X-axis indicate the final year of any temporal window over which the trend is calculated, and Y-axis indicate the window length.

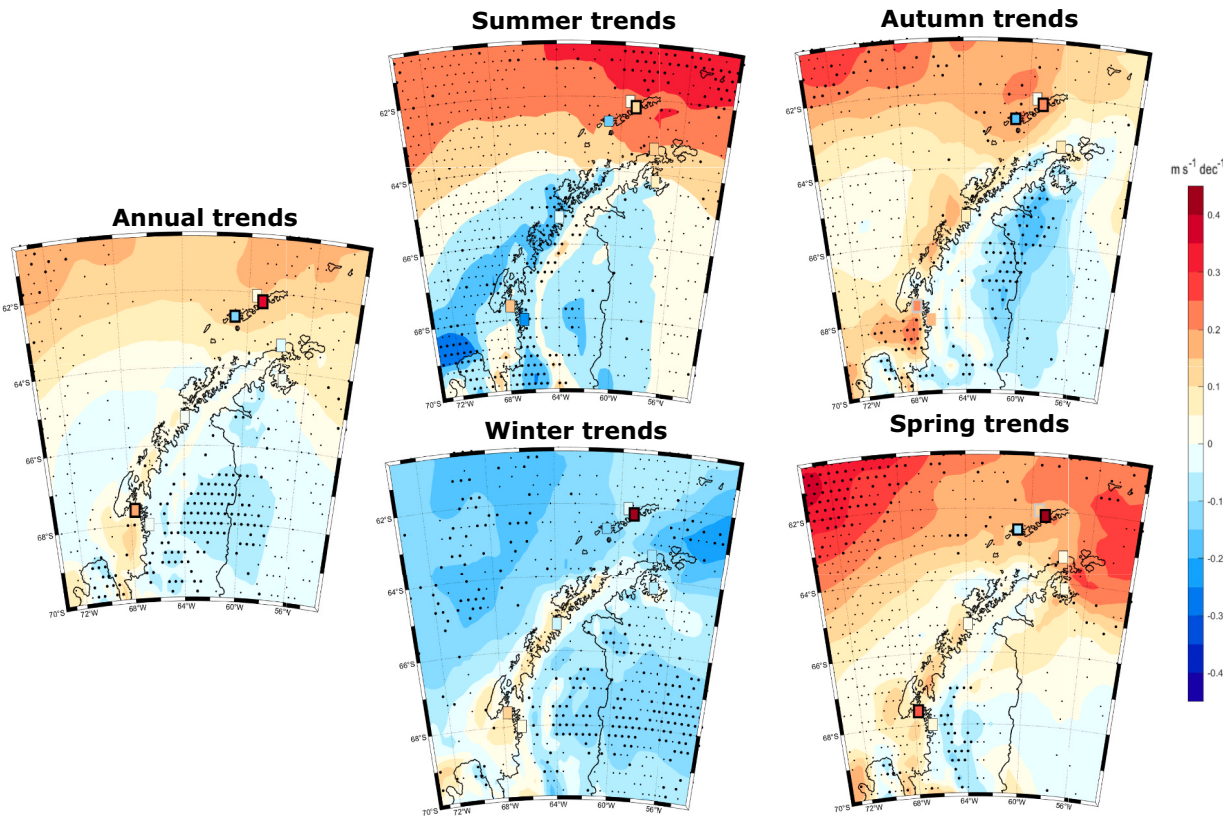

Fig. 6. Annual and seasonal spatial distribution of the SWS anomaly trends (m s^{-1} dec^{-1}) for 1979–2022 (1988–2022 for JCI). Statistical significance: large dots at $p < 0.05$ and small dots at $p < 0.10$ in the center of the grid-cells for ERA5 trends; black contour boxes at $p < 0.05$ and grey contour boxes at $p < 0.10$ for observational trends.

observed and reanalyzed SWS anomalies in the observation locations, excluding JCI, which covers a different time period (see Fig. S2). Generally, ERA5 shows a good agreement in reproducing the multi-decadal variability, especially in summer and spring, where the reanalysis accurately reflects the observed changes over the past decade. The identification of significant breakpoints (denoting shifts in trends) varies across time scales: starting in 1993 for spring, between 1999 and 2003 for summer, winter and annually, and in 2007 for autumn.

Moreover, the 10-yr Gaussian low-pass filter for the regional SWS anomalies shows a positive trend before the breakpoint and a cessation of this tendency after ~2001. Spring is the exception to this pattern, pointing to a continuous positive trend for the whole study period. Particularly, a remarkable oscillation is observed over the last decade during summer, where the decline period leads to a SWS reinforcement over the last 3 years. Additionally, comparing both data sources, annual and seasonal observed anomalies exhibit higher variability than ERA5 ones. Overall, ERA5 can capture the observed regional mean multi-decadal variability and trends. Contrary, for JCI (see Fig. S2) large differences appear, indicating the reanalysis's limitations in reproducing the SWS variability in JCI. Note that Fig. S2 represents only one station, while Fig. 4 displays the regional mean across the remaining observatories. These two figures cannot be directly compared, and it is expected for Fig. S2 to exhibit more variability.

Fig. 5 shows that seasonal trends are higher in magnitude than the annual ones. The succession of periods of reinforcement and decline of SWS indicates a marked natural internal variability, which appears clearly illustrated in Esperanza or Marambio. In addition, a weak decline of SWS can be observed for the recent years over the stations (also exemplified regionally in Fig. 4), remarkable during summer, and specially for Faraday/Vernadsky and Marambio.

3.3. Spatial distribution of SWS trends

Fig. 6 shows the spatial distribution of annual and seasonal trends for both ERA5 and stations. Consistent with the findings illustrated in Fig. 3, certain observatories exhibit a similar trend compared to the reanalysis, while others (i.e., Marsh, Rothera and JCI) clearly show large differences. These maps reveal that annual trends exhibit weaker magnitudes compared to the seasonal ones, primarily because of the pronounced seasonal variability. Annually, non-statistically significant positive trends are found over southern Drake Passage and in a narrow strip windward of the mountains of the AP (e.g. Rothera and Faraday/Vernadsky). Bellingshausen and Weddell Seas, as well the AP mountains and the Larsen C ice shelf present negative trends, being more significant in the latter region ($p < 0.05$). Seasonally, trends show large differences. Summer presents a spatial pattern denoting a decline of wind speed on the western side of the AP (mostly significant at $p < 0.05$) and an increase on the northern tip of the AP and over the South Shetland Islands. A different pattern is found in autumn, with positive trends in the western and northern side of the AP and negative ones in the leeward side of the peninsula ($p < 0.05$ near the Larsen C ice shelf). Spring exhibits a similar pattern compared to autumn, but just denoting negative trends in a reduced region over the leeward side of the mountain barrier and Weddell Sea. Lastly, negative trends dominate in winter across the AP ($p < 0.10$, over the northeast), with the exception of a narrow strip windward of the AP mountains (not significant). For all time scales except summer, a clear dipole of trends appears for the windward (positive) and leeward (negative) sides.

3.4. Relationship between SWS and atmospheric modes of variability

Pearson correlations of SWS with the SAM index (Fig. 7 and Fig. S4) exhibit higher and more statistically significant values than with the SOI

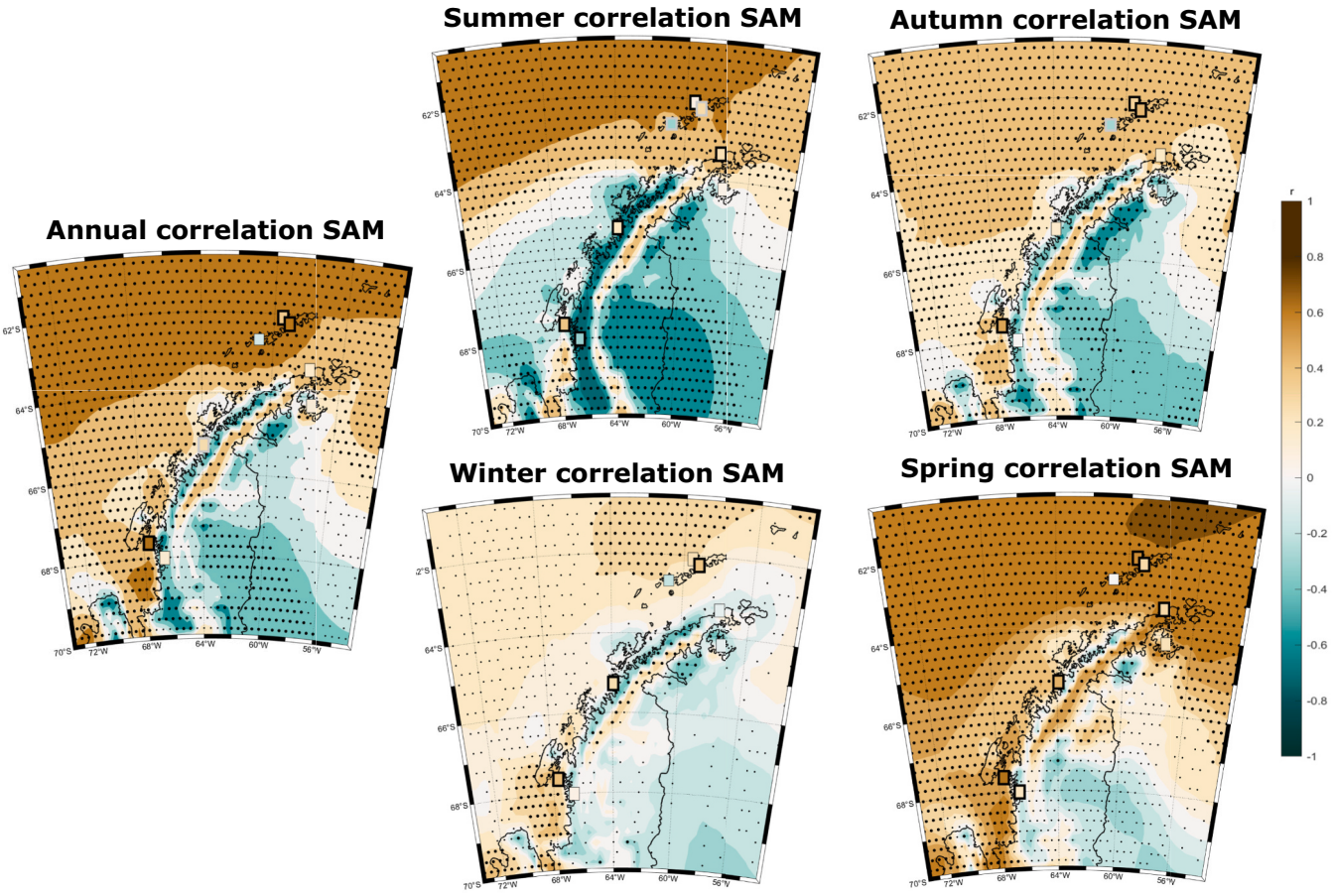

Fig. 7. Annual and seasonal Pearson correlation (r) and statistical significance between SWS anomalies and the SAM index for 1979–2022 (1988–2022 for JCI). Statistical significance: large dots at $p < 0.05$ and small dots at $p < 0.10$ in the centre of the grid-cells for ERA5; black contour boxes at $p < 0.05$ and grey contour boxes at $p < 0.10$ for observations.

index (Fig. 9 and Fig. S6), annually and seasonally. As the SAM index trend is positive (see supplementary Fig. S5), when the SWS increases, the correlation with SAM index is positive, and vice versa. Generally, we found that the correlations between SWS anomalies and indices are higher with ERA5 data than with the observations. Nevertheless, as shown in Fig. S5, the relationship between the SWS anomalies and the SAM index is non-stationary and complex. That is, the influence of the SAM index in the observed SWS varies depending on the selected time period. As an example, in winter between ~2009 and ~2013 the relationship is direct and strong, whereas no significant relationship occur between ~2014 and ~2020.

The regional observed SWS series (see supplementary Fig. S4) suggests a strong and significant positive correlation with the SAM index annually and in autumn and spring ($r = 0.50$, $r = 0.33$ and $r = 0.54$ respectively; $p < 0.05$). In addition, Marsh and Rothera are the stations denoting the highest correlations with the SAM index annually ($r = 0.61$ and $r = 0.69$; $p < 0.05$, respectively), whereas JCI is the only one displaying a weak annual negative correlation. Seasonally, spring presents the strongest and most statistically significant ($p < 0.05$) positive correlations for all stations (except JCI), showing a linear relationship between SWS and SAM. Although there is a good agreement between observations and the ERA5 nearest/vicinity grid points, some stations present discrepancies. For example, Marsh or Bellingshausen display similar results for both datasets, while Faraday/Vernadsky or Rothera present differences.

The spatial distribution of the annual and seasonal correlations between SAM and ERA5 SWS anomalies is shown in Fig. 7, presenting a clear pattern similar to SWS trends (Fig. 6): positive correlations ($p <$ 0.05 for all time periods except winter) are found in the northern tip of the AP and the South Shetland Islands; negative correlations are found over the eastern AP in the Larsen Ice Shelf ($p < 0.05$); seasonal differences appear over the western AP, with negative correlations in summer ($p < 0.10$), weaker positive correlations in winter, and positive in autumn and particularly in spring ($p < 0.05$). Two narrow stripes over the AP mountain range reveal a dipolar pattern with positive correlations over the windward side of the mountain barrier (western side), and negative correlations on the leeward side (eastern) for all time scales, being remarkable in summer and autumn.

Fig. 8 depicts the MSLP and SWS anomalies for the SAM+ and SAM- composites. The annual SAM+ composite denotes positive and statistically significant ($p < 0.05$) SWS anomalies in the westerly circumpolar belt across the Drake Passage, accompanied by marked negative MSLP anomalies over the ASL. In addition, negative anomalies with a northeastern component affect the eastern side and Larsen Ice Shelf. Summer SWS and MSLP anomalies are mostly weak (not significant) for both SAM+ and SAM- composites. During winter, under SAM+ composites, positive SWS anomalies are observed over the westerly belt, and the ASL experiences a deepening, although anomalies over the AP are relatively weak. In autumn and, particularly, in spring ($p < 0.05$), the SAM+ composite shows positive and statistically significant SWS anomalies over the northern and western side of the AP and a deepening of the ASL is detected.

Correlations between the SOI index and SWS anomalies are weak in all the stations and regional mean, but with low statistical significance (Fig. 9 and Fig. S6). For the observations, there is a dominance of positive r values, with the highest one in Rothera with $r = 0.39$ ($p < 0.05$) in

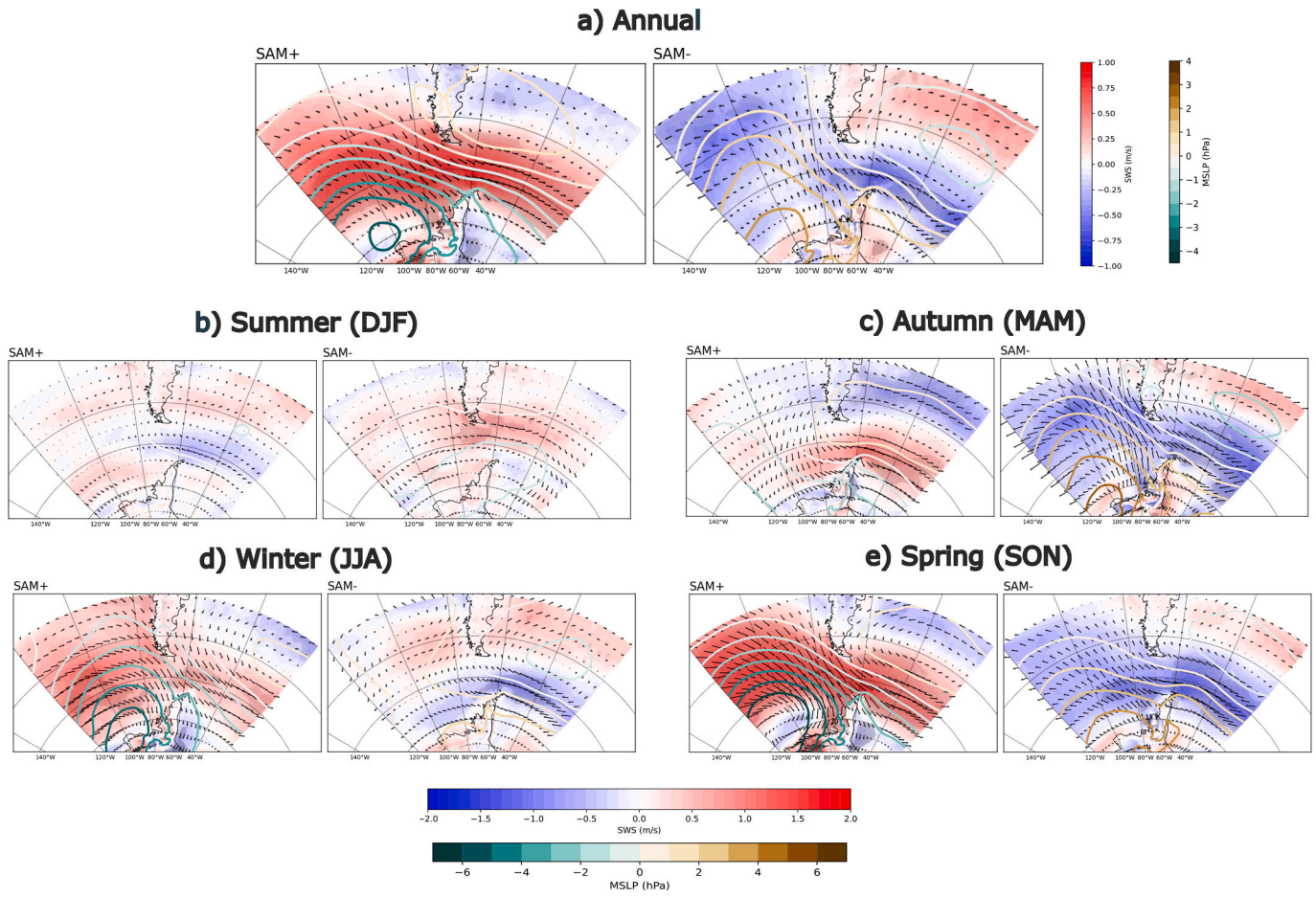

Fig. 8. Annual and seasonal SWS, MSLP and wind direction anomalies for SAM+ and SAM- composites. Notice that the colorbars range differs between the annual and seasonal plots. In all composites, anomalies statistically different from zero at $p < 0.05$ are shaded. The vectors show the direction and strength of the SWS anomalies.

spring. For ERA5, weak positive r values dominate annually and in summer and spring, while weak negative ones are more common in autumn and winter. The maps in Fig. 9 show a common spatial pattern ($p < 0.05$) for all time scales: positive correlations are observed on the western coast on the windward side of the AP mountain barrier, and negative ones on the leeward side and over the Weddell Sea. In addition, the northern tip of the AP and the South Shetland Islands exhibit positive statistically significant correlations ($p < 0.05$) for summer and weak results for the rest of the seasons. The SOI composites appear in Fig. 10. ENSO notably affects the ASL. During SOI+ composites (La Niña phases), the ASL experiences a deepening, strengthening SWS over the western AP across all time scales.

4. Discussion

This study investigates for the first time the spatio-temporal trends and multidecadal variability of SWS over the northern AP for 1979–2022, and its association with two main atmospheric circulation mechanisms: the SAM and the ENSO. We used two wind data sources: (i) 8 quality controlled and homogenized observational series, i.e., 7 stations from the SCAR MET-READER project, and the JCI station (1988–2022) which has been analyzed for the first time; and (ii) ERA5 reanalysis dataset.

4.1. ERA5 evaluation

The first part of this research explored the performance of ERA5 in reproducing the SWS over the stations. Negative MB are found for all stations, suggesting an underestimation of SWS by ERA5 and confirming the results of Tetzner et al. (2019), Dong et al. (2020), Nygård et al. (2016), Gossart et al. (2019) or Caton Harrison et al. (2022). The primary cause of the discrepancies between ERA5 and observations relies in the local processes forced by the complex terrain (i.e. foehn and barrier winds), which ERA5 fails to accurately reproduce (Caton Harrison et al., 2022; Dong et al., 2020; Minola et al., 2021; Nygård et al., 2016; Tetzner et al., 2019). Moreover, Van Wessem et al. (2015) pointed out that even using RACMO2.3 with a finer horizontal resolution of 5.5 km, the model cannot adequately represent the complex topography of the AP and the wind regimes.

Some authors found seasonal variations in the ability of reanalysis to reproduce SWS over the study area (e.g. Dong et al., 2020; Sanz Rodrigo et al., 2013; Tetzner et al., 2019). This might be explained because SWS does not only depend on the circulation, but on the stability and roughness effects, since it is the wind measured in the boundary layer (Wever, 2012; Wieringa, 1989) and these processes are still not well reproduced in the current reanalysis (Peng et al., 2022). Stability varies due to the different buoyancy effect by warm and cold air and the blocking effect by the mountains. Roughness also might change due to the seasonal sea ice in the area. In our results, although weak seasonal variations are observed in the statistics, the dominant factor affecting ERA5 performance is the station-dependence, caused by discrepancies between results obtained from different observatories (i.e. good performance over Bellingshausen or March, poor results over Rothera or JCI). A plausible explanation could be related to differences between the location of weather stations and the selected reanalysis grid points or grid averages (Gossart et al., 2019). As the AP presents a rough

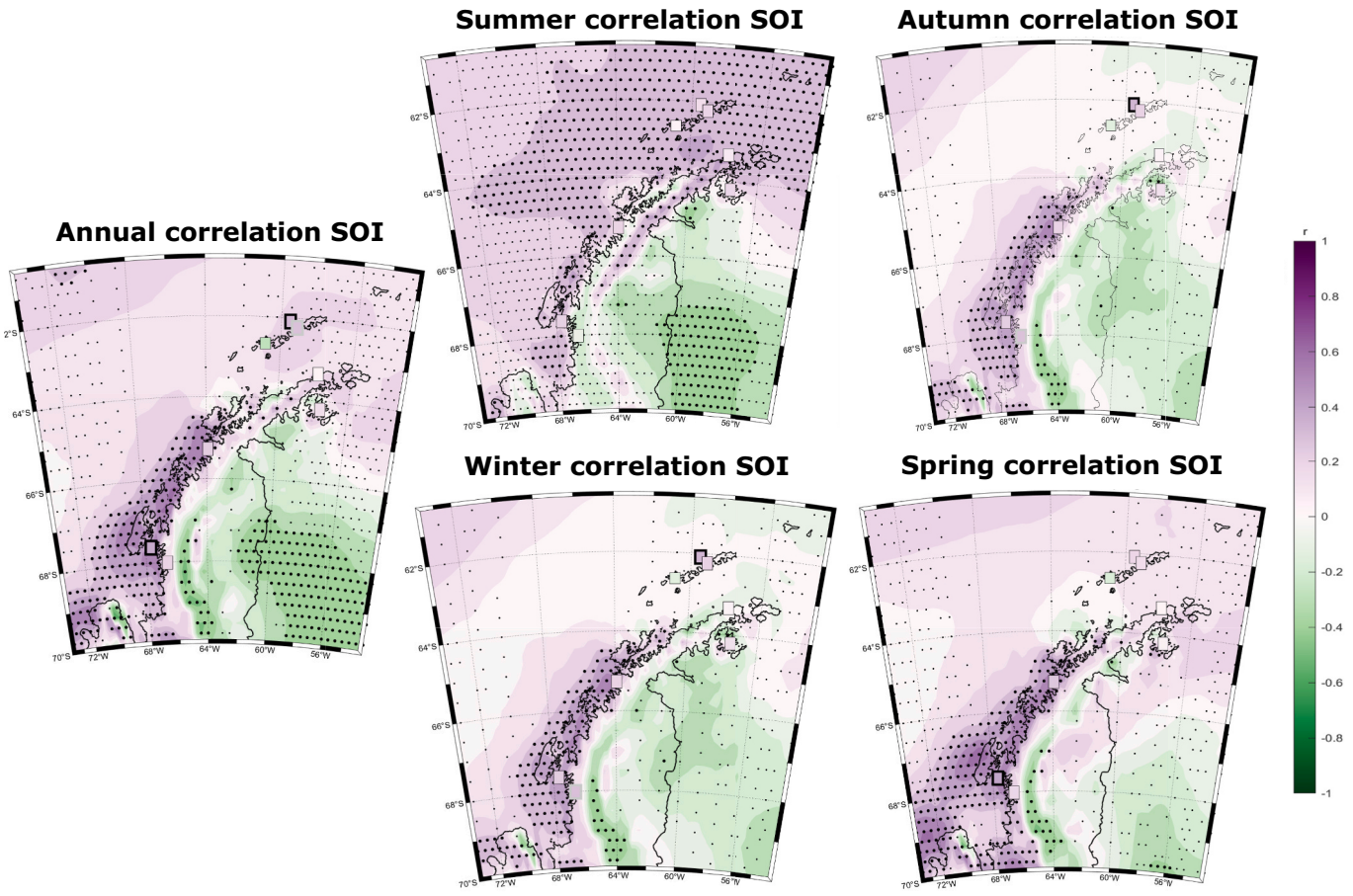

Fig. 9. As Fig. 7 but for the SOI.

orography, the nearest grid point could correspond to an offshore location or a point with different terrain features, leading to biases (Gossart et al., 2019). The poor performance of JCI can illustrate this hypothesis. JCI is located in a sheltered area, protected against strong winds from the north-east (Bañón et al., 2013). The mountain barrier behind the station (i.e. Mount Reina Sofia) helps to block winds, generating discrepancies between the station and ERA5 gridded data. This explanation is similar to the one suggested by Evtushevsky et al. (2020) for Faraday/Vernadsky; they pointed out that the mountains to the east of the station act as a barrier for zonal circulations, generating large variability and weaker winds compared to Esperanza, located close by. In addition to the mountain barrier, cold, dense and stable air piled up against the slopes of the mountains (Parish, 1983; Schwerdtfeger, 1975), generate a locally stable atmosphere (Nygård et al., 2016), that could weaken the winds.

The number of observatories over the AP is limited (Caton Harrison et al., 2022; Wang et al., 2021), and stations are located in areas protected against the harsh environmental conditions (Evtushevsky et al., 2020; Tardif et al., 2022). This could play a key role in understanding the SWS changes and variability of the observational data. Nevertheless, the regional mean (without JCI due to the different study period) suggests good correlations between stations and the reanalysis. In addition, ERA5 denotes good abilities in reproducing the multidecadal variability and trends, indicating that the reanalysis can reproduce the general wind speed temporal variability. As proposed by Azorin-Molina et al. (2014), although the local features of wind speed are expressed in observational data, they also represent the changes in large-scale atmospheric circulation (Azorin-Molina et al., 2014). The number of Automatic Weather Stations has grown up since the 1980s, but there are still significant gaps in the heterogeneous Antarctic network (Wang et al., 2023). The harsh conditions of the continent make it difficult to maintain the station network (Wang et al., 2021). As climate models actually cannot represent SWS with enough accuracy (Shen et al., 2022), the use of observations continues to be crucial and are the backbone of wind research (Utrabo-Carazo et al., 2022). In order to reduce efforts, it will be crucial to optimize the network by setting up stations in representative areas (González et al., 2021; Tardif et al., 2022). Since observed SWS data are not assimilated (only SWS data from satellites and radar are used), incorporating these observations improve the simulation of SWS by the reanalysis. This would strongly help to improve future climate studies in the AP.

4.2. SWS trends and ocean-atmosphere leading modes

Across all time scales, for both observations and ERA5, generally strong positive trends are directly and significantly correlated with the SAM index, although there are some exceptions (e.g., Marsh). Additionally, as a general rule, the stronger the trend, the stronger the correlation. The observational regional mean indicates positive SWS trends for all time scales, being remarkable for spring $+0.151$ m s^{-1} dec^{-1} ($p <$ 0.05). The positive trend of the SAM index has been attributed to two main reasons: first, the polar stratospheric ozone depletion (Banerjee et al., 2020; Fogt and Marshall, 2020); and in second place, the increase in greenhouse gasses (Deng et al., 2022; Fogt and Marshall, 2020). Given the positive correlations of SWS with the SAM index, the enhanced synoptic winds driven by the poleward shift of the circumpolar westerly belt (Marshall, 2007; Thompson and Solomon, 2002), which produces positive SWS anomalies over the study region, could be behind the general strengthening of SWS (Dong et al., 2020).

In addition, the temporal variability analysis reveals a reduction in

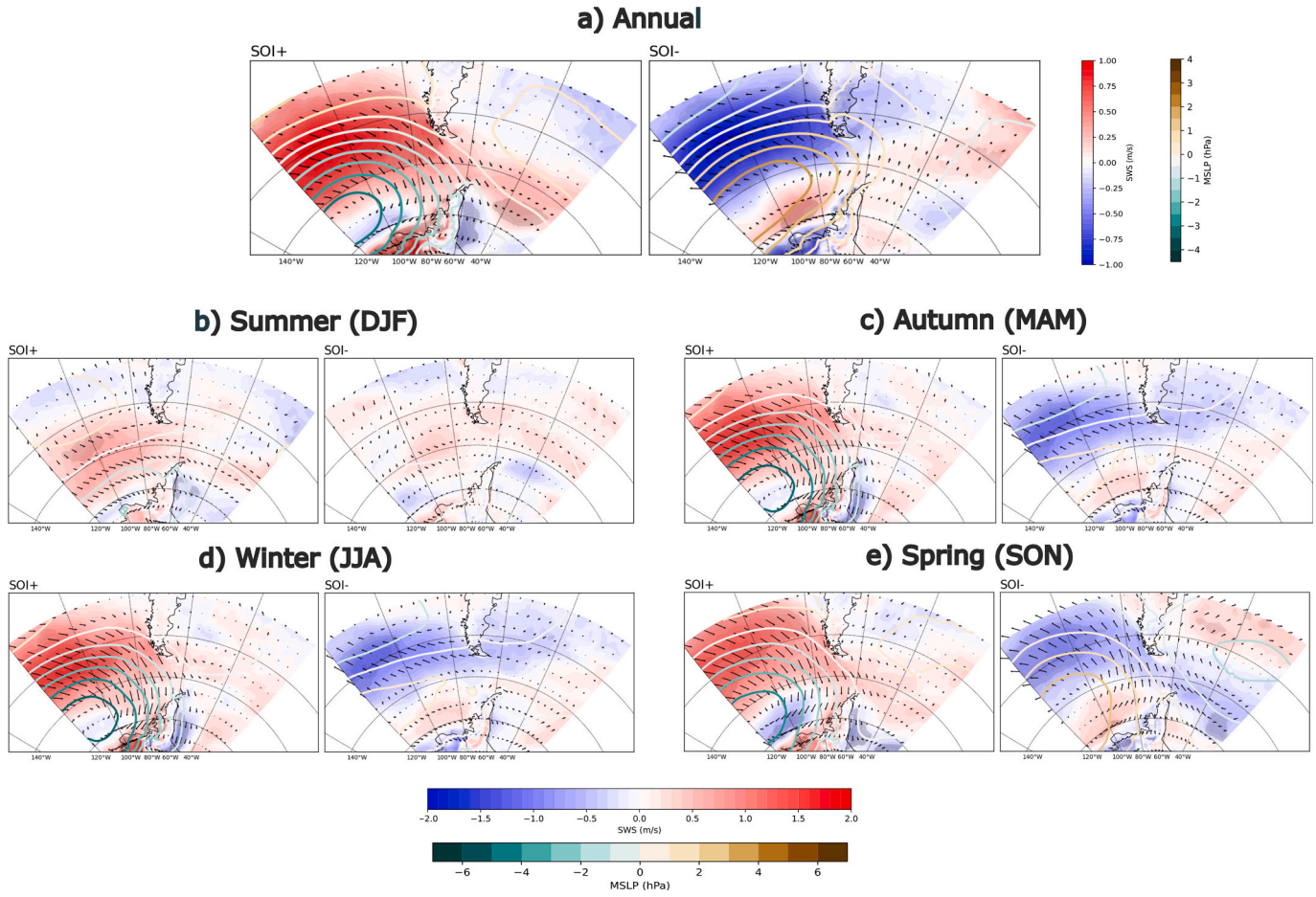

Fig. 10. As Fig. 8 but for the SOI.

SWS since ~2001, particularly during summer. The succession of periods of reinforcement and decline denotes a strong internal variability of SWS. Recent studies suggest that ocean-atmosphere oscillations are the main cause behind this multidecadal variability of SWS (Zeng et al., 2019), which is in agreement with our results. Here, we show that the SAM plays a major role, while ENSO is secondary over the long time span. The relationship between the SAM index and air temperature, precipitation or other proxies is non-stationary (Gallant et al., 2013; King et al., 2023; Silvestri and Vera, 2009), varying significantly over time. Similarly, our study shows that the influence of the SAM index on SWS over the AP is also non-stationary and complex. SWS could be also influenced by spatial changes in the SAM structure (Fogt and Marshall, 2020), changes in atmospheric stability (Zapponini and Goessling, 2024), connection with ENSO (Goodwin et al., 2016; Raphael et al., 2016), anthropogenic forcing and greenhouse concentration (King et al., 2023) or stratospheric ozone (Banerjee et al., 2020), among others.

Other possible causes behind wind changes could be associated with the anemometer performance (Azorin-Molina et al., 2018b); for instance, anemometers might usually freeze in the AP (Gossart et al., 2019). The increase in surface roughness proposed by Vautard et al. (2010) would play a marginal role over the AP, where land-use changes might be of minor relevance. However, changes in the surface roughness might occur due to modification in sea ice and ice sheets extent and might affect the SWS (Liu et al., 2024). Quantifying the role of all these factors is out of the scope of this article but should be explored in the future.

4.3. Spatial patterns

Taking into account the observations, it is not possible to extract a clear spatial pattern of SWS trends due to the limited availability of stations and the control exerted by local processes. Given the previously discussed limitations of ERA5 in reproducing the observed SWS, the spatial pattern of SWS trends should be interpreted with caution. However, in ERA5 we found a dominance of positive SWS trends over the southern Drake Passage and South Shetland Islands, except for winter. Given the positive SWS anomalies and its strong correlation ($p < 0.05$) with the SAM index, the poleward shift of the westerly belt might be the main driver behind the SWS strengthening, confirming the findings of Thompson and Solomon (2002), Marshall (2007) or Deng et al. (2022).

Over the eastern AP and Larsen Ice Shelf, in general negative trends appear. This region is characterized by strong barrier winds: southwesterly winds generated by cold air from the continent, accumulated against the AP mountain due to its static stability (i.e. "damming up" effect), lead to pressure gradients, which generates these barrier winds (Parish, 1983). Under the SAM+ composites, the SWS anomalies are negative and with a north-eastern component, which could affect the barrier winds over the eastern AP and Larsen Ice Shelf, thereby generating negative trends in SWS. In other words, as the SAM index trends increase, a reduction of SWS over the eastern side could be expected. This effect could have key implications on the ice shelf stability leading to two counteracting forcings. On one hand, the reduction of cold southwesterly winds lead to warmer temperatures contributing to more surface melting. On the other hand, it decreases the wind stress over the ice and the waves that induce fractures on the ice shelf.

For autumn and spring, the relationship between the SAM index and SWS appeared to be more direct, particularly over the western AP. Across the SAM+ composites, positive SWS anomalies are detected over the northern and western side of the AP, and a deepening of the ASL is noticeable (Clem et al., 2016, 2017; Fogt and Marshall, 2020). During these seasons, the correlation between SWS anomalies and the the SOI index is also strong, suggesting that the ENSO and its teleconnection with the ASL plays a pivotal role (Clem et al., 2016; Clem and Fogt, 2013; Fogt et al., 2012). During La Niña (El Niño) conditions, the ASL suffers a deepening (filling) (Clem et al., 2016), strengthening (weakening) the northerly winds over the western AP (Hosking et al., 2013). In spring, the ASL deepening and SWS anomalies are more pronounced than in autumn. Stronger winds can cross through the barrier generating foehn winds. This phenomenon might be an explanation of why in the north-east side of the AP positive SWS trends are observed during spring but not during autumn.

Summer SWS and MSLP anomalies are mostly weak (not significant) for both SAM+ and SAM- composites. The literature reflects (e.g. Fogt and Marshall, 2020) that during summer the positive trend of SAM is remarkable (also noticeable in Fig.S5), so positive SWS anomalies should be expected. This a perfect example of how the relationship between SAM and SWS is non-stationary and modulated by other dynamic and climatic factors. In winter, under the SAM+ composites, the SWS anomalies are mostly negative. Considering that the SAM index does not present a positive trend in this season and SWS trends are negative over the region, other mechanisms might be behind the negative trends shown in Fig. 6. Further research is needed to attribute the causes behind this change.

4.4. Further research

Next research steps should focus on understanding the interaction between winds, orography and the main modes of climate variability, from a local to regional point of view, to understand and attribute the SWS trends and multidecadal variability. As winds are measured in the atmospheric boundary layer in a very complex region, the interplay between roughness length, stability and orography might determine the changes on SWS. Also, we should deepen our knowledge on the control exerted by the principal modes of variability. Particularly, this study shows how the interactions between the SAM index and the SWS is non-stationary and complex. A better understanding of this interactions will help to attribute the SWS changes. In addition, the effect of other modes of variability that play a role over timescales ranging from months to decades, such as the Pacific Interdecadal Oscillation or the SemiAnnual Oscillation, should be studied. Lastly, but not less important, further research should focus on the impact of global warming on the stability and SWS (Liu et al., 2024). As the AP, particularly the west coast, is warming at a faster rate than the global average (González-Herrero et al., 2024), a reduction of the stability and an increase in SWS could be expected during the 21st century (Zapponini and Goessling, 2024).

5. Conclusion

The principal findings of this research are:

1. The observed positive trend in SWS in the first decades has been followed by a period of decline in SWS since ~2001, which has been reported for the first time. The general observed positive trends exhibit a strong interannual variability, with a remarkable SWS reinforcement during autumn and, particularly, in spring.
2. The general positive trends in observed SWS, mainly over the South Shetland Island and the Drake Passage, could be partly associated with the increase and poleward shift of the westerlies due to the positive trend of the SAM index for 1979–2022.
3. The spatial trend patterns retrieved from ERA5 show negative trends over the eastern AP and the Larsen Ice Shelves which could be associated with a weakening in barrier winds; while the positive trends (spring and autumn) in the western AP could be partly driven by the deepening of the ASL associated to the teleconnection of ENSO and the positive trend of SAM.
4. These evidences reveal that the relationship between SWS and the SAM index is non-stationary and complex. For instance, despite the strongest positive trend of the SAM occurred in summer, the major significant role of this index is exerted in autumn and, especially, spring. Other causes such as the structure of the SAM, atmospheric stability, anthropogenic forcing, etc., might be behind the observed SWS changes and variability, and future attribution studies are strongly needed to discern the complex responses of SWS to different drivers.

CRediT authorship contribution statement

Miguel Andres-Martin: Writing – original draft, Software, Methodology, Formal analysis, Conceptualization. **Cesar Azorin-Molina:** Writing – review & editing, Supervision, Resources, Funding acquisition, Conceptualization. **Encarna Serrano:** Writing – review & editing, Supervision. **Sergi González-Herrero:** Writing – review & editing, Supervision, Conceptualization. **Jose A. Guijarro:** Writing – review & editing, Resources, Data curation. **Shalenys Bedoya-Valestt:** Writing – review & editing. **Eduardo Utrabo-Carazo:** Writing – review & editing. **Sergio M. Vicente Serrano:** Writing – review & editing.

Declaration of competing interest

The authors declare no conflict of interest.

Data availability

Wind speed data from stations observations were obtained from AEMET (Juan Carlos I base station data, available upon request to the corresponding author) and SCAR MET-READER project (publicly available at https://legacy.bas.ac.uk/met/READER/data.html). Monthly ERA5 wind speed data was retrieved from Copernicus Climate Data Store (https://cds.climate.copernicus.eu/#!/search?text=ERA5&type=dataset). Station-based SAM index developed by Marshall was downloaded from https://legacy.bas.ac.uk/met/gjma/sam.html, and SOI index from NOAA are available online at https://www.ncdc.noaa.gov/teleconnections/enso/indicators/soi/.

Acknowledgments

We thank all the staff of the different stations on the Antarctic Peninsula for their work in the installation and maintenance of the weather stations. In particular, we want to acknowledge Manuel Bañón, who was responsible of the weather station at the Spanish Base Station Juan Carlos I, and also for the exchange of his knowledge on winds over the Antarctica. This research was funded by the following projects: IBER-STILLING (RTI2018-095749-A-I00, MCIU/AEI/FEDER,UE); VENTS (GVA-AICO/2021/023) and the CSIC Interdisciplinary Thematic Platform (PTI) Clima (PTI+ CLIMA). M. A-M was supported with a FPU grant (FPU21/03748) from the “Ministerio de Universidades”. M. A-M. and C.A-M were supported by a 2021 Leonardo Grant for Researchers and Cultural Creators, BBVA Foundation. S.G. was supported by ANT-ALP Research Group, Generalitat de Catalunya. This study is also supported by “Unidad Asociada CSIC-Universidad de Vigo: Grupo de Fisica de la Atmósfera y del Océano”. The authors wish to acknowledge the anonymous reviewers for their detailed and helpful comments to the original manuscript.

Appendix A. Supplementary data

Supplementary data to this article can be found online at https://doi.

org/10.1016/j.atmosres.2024.107568.

References

Alexandersson, H., 1986. A homogeneity test applied to precipitation data. J. Climatol. 6 (485).

Azorin-Molina, C., Vicente-Serrano, S.M., Mcvicar, T.R., Jerez, S., Sanchez-Lorenzo, A., López-Moreno, J.I., Revuelto, J., Trigo, R.M., Lopez-Bustins, J.A., Espírito-Santo, F., 2014. Homogenization and assessment of observed near-surface wind speed trends over Spain and Portugal, 1961-2011. J. Clim. 27 (10), 3692–3712. https://doi.org/10.1175/JCLI-D-13-00652.1.

Azorin-Molina, C., Guijarro, J.A., McVicar, T.R., Vicente-Serrano, S.M., Chen, D., Jerez, S., Espírito-Santo, F., 2016. Trends of daily peak wind gusts in Spain and Portugal, 1961–2014. J. Geophys. Res. 121 (3), 1059–1078. https://doi.org/10.1002/2015JD024485.

Azorin-Molina, C., Asin, J., McVicar, T.R., Minola, L., Lopez-Moreno, J.I., Vicente-Serrano, S.M., Chen, D., 2018a. Evaluating anemometer drift: a statistical approach to correct biases in wind speed measurement. Atmos. Res. 203 (November 2017), 175–188. https://doi.org/10.1016/j.atmosres.2017.12.010.

Azorin-Molina, C., Rehman, S., Guijarro, J.A., McVicar, T.R., Minola, L., Chen, D., Vicente-Serrano, S.M., 2018b. Recent trends in wind speed across Saudi Arabia, 1978–2013: a break in the stilling. Int. J. Climatol. 38, e966–e984. https://doi.org/10.1002/joc.5423.

Banerjee, A., Fyfe, J.C., Polvani, L.M., Waugh, D., Chang, K.L., 2020. A pause in Southern Hemisphere circulation trends due to the Montreal Protocol. Nature 579 (7800), 544–548. https://doi.org/10.1038/s41586-020-2120-4.

Bañón, M., Justel, A., Velázquez, D., Quesada, A., 2013. Regional weather survey on byers peninsula, Livingston island, south shetland islands, Antarctica. Antarct. Sci. 25 (2), 146–156. https://doi.org/10.1017/S0954102012001046.

Bozkurt, D., Rondanelli, R., Marín, J.C., Garreaud, R., 2018. Foehn event triggered by an atmospheric river underlies record-setting temperature along Continental Antarctica. J. Geophys. Res. Atmos. 123 (8), 3871–3892. https://doi.org/10.1002/2017JD027796.

Brunetti, M., Maugeri, M., Nanni, T., Auer, I., Böhm, R., Schöner, W., 2006. Precipitation variability and changes in the greater Alpine region over the 1800-2003 period. J. Geophys. Res. Atmos. 111 (11) https://doi.org/10.1029/2005JD006674.

Cape, M.R., Vernet, M., Skvarca, P., Marinsek, S., Scambos, T., Domack, E., 2015. Foehn winds link climate-driven warming to ice shelf evolution in Antarctica. J. Geophys. Res. 120 (21), 11,037–11,057. https://doi.org/10.1002/2015JD023465.

Carrasco, J.F., Bozkurt, D., Cordero, R.R., 2021. A review of the observed air temperature in the Antarctic Peninsula. Did the warming trend come back after the early 21st hiatus? Polar Sci. February, 100653 https://doi.org/10.1016/j.polar.2021.100653.

Caton Harrison, T., Biri, S., Bracegirdle, T.J., King, J.C., Kent, E.C., Vignon, É., Turner, J., 2022. Reanalysis representation of low-level winds in the Antarctic near-coastal region. Weather Clim. Dynam. 3 (4), 1415–1437. https://doi.org/10.5194/wcd-3-1415-2022.

Clem, K.R., Fogt, R.L., 2013. Varying roles of ENSO and SAM on the Antarctic Peninsula climate in austral spring. J. Geophys. Res. Atmos. 118 (20), 11,481–11,492. https://doi.org/10.1002/jgrd.50860.

Clem, K.R., Renwick, J.A., Mcgregor, J., Fogt, R.L., 2016. The relative influence of ENSO and SAM on Antarctic Peninsula climate. Nature 175 (4449), 238. https://doi.org/10.1038/175238c0.

Clem, K.R., Renwick, J.A., Mcgregor, J., 2017. Large-scale forcing of the Amundsen Sea low and its influence on sea ice and west antarctic temperature. J. Clim. 30 (20), 8405–8424. https://doi.org/10.1175/JCLI-D-16-0891.1.

Deng, K., Azorin-Molina, C., Yang, S., Hu, C., Zhang, G., Minola, L., Chen, D., 2022. Changes of Southern Hemisphere westerlies in the future warming climate. Atmos. Res. 270 https://doi.org/10.1016/j.atmosres.2022.106040.

Dong, X., Wang, Y., Shugui, H.O.U., Ding, M., Baoling, Y.I.N., Zhang, Y., 2020. Robustness of the recent global atmospheric reanalyses for antarctic near-surface wind speed climatology. J. Clim. 33 (10), 4027–4043. https://doi.org/10.1175/JCLI-D-19-0648.1.

Elvidge, A.D., Kuipers Munneke, P., King, J.C., Renfrew, I.A., Gilbert, E., 2020. Atmospheric drivers of melt on larsen C ice shelf: surface energy budget regimes and the impact of Foehn. J. Geophys. Res. Atmos. 125 (17) https://doi.org/10.1029/2020JD032463.

Evtushevsky, O.M., Kravchenko, V.O., Grytsai, A.V., Milinevsky, G.P., 2020. Winter climate change on the northern and southern Antarctic Peninsula. Antarct. Sci. 32 (5), 408–424. https://doi.org/10.1017/S0954102020000255.

Fan, W., Liu, Y., Chappell, A., Dong, L., Xu, R., Ekström, M., Fu, T.M., Zeng, Z., 2020. Evaluation of global reanalysis land surface wind speed trends to support wind energy development using in situ observations. J. Appl. Meteorol. Climatol. 60 (1), 33–50. https://doi.org/10.1175/JAMC-D-20-0037.1.

Fogt, R.L., Marshall, G.J., 2020. The Southern Annular Mode: Variability, trends, and climate impacts across the Southern Hemisphere. Wiley Interdiscip. Rev. Clim. Chang. 11 (4), 1–24. https://doi.org/10.1002/wcc.652.

Fogt, R.L., Wovrosh, A.J., Langen, R.A., Simmonds, I., 2012. The characteristic variability and connection to the underlying synoptic activity of the Amundsen-Bellingshausen Seas Low. J. Geophys. Res. Atmos. 117 (7) https://doi.org/10.1029/2011JD017337.

Gallant, A.J.E., Phipps, S.J., Karoly, D.J., Mullan, A.B., Lorrey, A.M., 2013. Nonstationary Australasian teleconnections and implications for paleoclimate reconstructions. J. Clim. 26 (22), 8827–8849. https://doi.org/10.1175/JCLI-D-12-00338.1.

Gonzalez, S., Vasallo, F., Recio-Blitz, C., Guijarro, J.A., Riesco, J., 2018. Atmospheric patterns over the Antarctic Peninsula. J. Clim. 31 (9), 3597–3608. https://doi.org/10.1175/JCLI-D-17-0598.1.

González, S., Vasallo, F., Sanz, P., Quesada, A., Justel, A., 2021. Characterization of the summer surface mesoscale dynamics at Dome F, Antarctica. Atmos. Res. 259 https://doi.org/10.1016/j.atmosres.2021.105699.

González-Herrero, S., Barriopedro, D., Trigo, R.M., López-bustins, J.A., 2022. Climate warming ampli fi ed the 2020 record-. Idl, pp. 1–9. https://doi.org/10.1038/s43247-022-00450-5.

González-Herrero, S., Navarro, F., Pertierra, L.R., Oliva, M., Dadic, R., Peck, L., Lehning, M., 2024. Southward migration of the zero-degree isotherm latitude over the Southern Ocean and the Antarctic Peninsula: Cryospheric, biotic and societal implications. Sci. Total Environ. 912 https://doi.org/10.1016/j.scitotenv.2023.168473.

Goodwin, B.P., Mosley-Thompson, E., Wilson, A.B., Porter, S.E., Roxana Sierra-Hernandez, M., 2016. Accumulation variability in the Antarctic Peninsula: the role of large-scale atmospheric oscillations and their interactions*. J. Clim. 29 (7), 2579–2596. https://doi.org/10.1175/JCLI-D-15-0354.1.

Gossart, A., Helsen, S., Lenaerts, J.T.M., Vanden Broucke, S., van Lipzig, N.P.M., Souverijns, N., 2019. An evaluation of surface climatology in state-of-the-art reanalyses over the Antarctic Ice Sheet. J. Clim. 32 (20), 6899–6915. https://doi.org/10.1175/JCLI-D-19-0030.1.

Guijarro, J.A., 2018. Homogenization of Climatological Series with Climatol Version 3.1.1. 1(August), p. 20.

Hamed, K.H., Rao, A.R., 1998. Hydrology a modified Mann-Kendall trend test for autocorrelated data. J. Hydrol. 204.

Hersbach, H., Bell, B., Berrisford, P., Hirahara, S., Horányi, A., Muñoz-Sabater, J., Nicolas, J., Peubey, C., Radu, R., Schepers, D., Simmons, A., Soci, C., Abdalla, S., Abellan, X., Balsamo, G., Bechtold, P., Biavati, G., Bidlot, J., Bonavita, M., Thépaut, J.N., 2020. The ERA5 global reanalysis. Q. J. R. Meteorol. Soc. 146 (730), 1999–2049. https://doi.org/10.1002/qj.3803.

Holland, M.M., Landrum, L., Kostov, Y., Marshall, J., 2017. Sensitivity of Antarctic Sea ice to the Southern Annular Mode in coupled climate models. Clim. Dyn. 49 (5–6), 1813–1831. https://doi.org/10.1007/s00382-016-3424-9.

Hosking, J.S., Orr, A., Marshall, G.J., Turner, J., Phillips, T., 2013. The influence of the amundsen-bellingshausen seas low on the climate of West Antarctica and its representation in coupled climate model simulations. J. Clim. 26 (17), 6633–6648. https://doi.org/10.1175/JCLI-D-12-00813.1.

IPCC, 2021. Climate change 2021: The physical science basis. In: Contribution of Working Group I To the Sixth Assessment Report of the Intergovernmental Panel on Climate Change. Cambridge University Press. In Press.

Jones, M.E., Bromwich, D.H., Nicolas, J.P., Carrasco, J., Plavcová, E., Zou, X., Wang, S. H., 2019. Sixty years of widespread warming in the southern middle and high latitudes (1957–2016). J. Clim. 32 (20), 6875. https://doi.org/10.1175/JCLI-D-18-0565.1.

King, J., Anchukaitis, K.J., Allen, K., Vance, T., Hessl, A., 2023. Trends and variability in the Southern Annular Mode over the Common Era. Nat. Commun. 14 (1) https://doi.org/10.1038/s41467-023-37643-1.

Laffin, M.K., Zender, C.S., van Wessem, M., Noël, B., Wang, W., 2023. Wind-associated melt trends and contrasts between the Greenland and Antarctic Ice Sheets. Geophys. Res. Lett. 50 (16) https://doi.org/10.1029/2023GL102828.

Liau, J.R., Chao, B.F., 2017. Variation of Antarctic circumpolar current and its intensification in relation to the southern annular mode detected in the time-variable gravity signals by GRACE satellite 6. Geodesy. Earth Planets Space 69 (1). https://doi.org/10.1186/s40623-017-0678-3.

Liu, W., Yang, S., Chen, D., Zha, J., Zhang, G., Zhang, Z., Zhang, T., Xu, L., Hu, X., Deng, K., 2024. Rapid acceleration of arctic near-surface wind speed in a warming climate. Geophys. Res. Lett. 51 (8) https://doi.org/10.1029/2024GL109385.

Marshall, G.J., 2002. Analysis of recent circulation and thermal advection change in the northern Antarctic Peninsula. Int. J. Climatol. 22 (12), 1557–1567. https://doi.org/10.1002/joc.814.

Marshall, G.J., 2003. Trends in the Southern Annular Mode from observations and reanalyses. J. Clim. 16 (24), 4134–4143. https://doi.org/10.1175/1520-0442(2003)016<4134:TITSAM>2.0.CO;2.

Marshall, G.J., 2007. Half-century seasonal relationships between the Southern Annular Mode and Antarctic temperatures. Int. J. Climatol. 27 (3), 373–383. https://doi.org/10.1002/joc.1407.

Marshall, G.J., Thompson, D.W.J., van den Broeke, M.R., 2017. The signature of southern hemisphere atmospheric circulation patterns in Antarctic precipitation. Geophys. Res. Lett. 44 (22), 11,580–11,589. https://doi.org/10.1002/2017GL075998.

McVicar, T.R., Roderick, M.L., Donohue, R.J., Li, L.T., Van Niel, T.G., Thomas, A., Grieser, J., Jhajharia, D., Himri, Y., Mahowald, N.M., Mescherskaya, A.V., Kruger, A. C., Rehman, S., Dinpashoh, Y., 2012. Global review and synthesis of trends in observed terrestrial near-surface wind speeds: implications for evaporation. J. Hydrol. 416–417, 182–205. https://doi.org/10.1016/j.jhydrol.2011.10.024.

Minola, L., Azorin-Molina, C., Chen, D., 2016. Homogenization and assessment of observed near-surface wind speed trends across Sweden, 1956-2013. J. Clim. 29 (20), 7397–7415. https://doi.org/10.1175/JCLI-D-15-0636.1.

Minola, L., Reese, H., Lai, H.W., Azorin-Molina, C., Guijarro, J.A., Son, S.W., Chen, D., 2021. Wind stilling-reversal across Sweden: the impact of land-use and large-scale atmospheric circulation changes. Int. J. Climatol. October, 1–23. https://doi.org/10.1002/joc.7289.

Muggeo, V.M.R., 2003. Estimating regression models with unknown break-points. Stat. Med. 22 (19), 3055–3071. https://doi.org/10.1002/sim.1545.

Muggeo, V.M.R., 2016. Testing with a nuisance parameter present only under the alternative: a score-based approach with application to segmented modelling. J. Stat.

Comput. Simul. 86 (15), 3059–3067. https://doi.org/10.1080/00949655.2016.1149855.
Nygård, T., Vihma, T., Birnbaum, G., Hartmann, J., King, J., Lachlan-Cope, T., Ladkin, R., Lüpkes, C., Weiss, A., 2016. Validation of eight atmospheric reanalyses in the Antarctic Peninsula region. Q. J. R. Meteorol. Soc. 142 (695), 684–692. https://doi.org/10.1002/qj.2691.
Oliva, M., Navarro, F., Hrbáček, F., Hernández, A., Nývlt, D., Pereira, P., Ruiz-Fernández, J., Trigo, R., 2017. Recent regional climate cooling on the Antarctic Peninsula and associated impacts on the cryosphere. Sci. Total Environ. 580, 210–223. https://doi.org/10.1016/j.scitotenv.2016.12.030.
Orr, A., Marshall, G.J., Hunt, J.C.R., Sommeria, J., Wang, C.G., van Lipzig, N.P.M., Cresswell, D., King, J.C., 2008. Characteristics of summer airflow over the Antarctic Peninsula in response to recent strengthening of Westerly circumpolar winds. J. Atmos. Sci. 65 (4), 1396–1413. https://doi.org/10.1175/2007JAS2498.1.
Parish, T.R., 1983. The influence of the Antarctic Peninsula on the wind field over the western Weddell Sea. J. Geophys. Res. 88 (C4), 2684. https://doi.org/10.1029/jc088ic04p02684.
Peng, Z., Tang, R., Jiang, Y., Liu, M., Li, Z.L., 2022. Global estimates of 500 m daily aerodynamic roughness length from MODIS data. ISPRS J. Photogramm. Remote Sens. 183, 336–351. https://doi.org/10.1016/j.isprsjprs.2021.11.015.
Ramon, J., Lledó, L., Torralba, V., Soret, A., Doblas-Reyes, F.J., 2019. What global reanalysis best represents near-surface winds? Q. J. R. Meteorol. Soc. 145 (724), 3236–3251. https://doi.org/10.1002/qj.3616.
Raphael, M.N., Marshall, G.J., Turner, J., Fogt, R.L., Schneider, D., Dixon, D.A., Hosking, J.S., Jones, J.M., Hobbs, W.R., 2016. The Amundsen Sea low: variability, change, and impact on Antarctic climate. Bull. Am. Meteorol. Soc. 97 (1), 111–121. https://doi.org/10.1175/BAMS-D-14-00018.1.
Roderick, M.L., Rotstayn, L.D., Farquhar, G.D., Hobbins, M.T., 2007. On the attribution of changing pan evaporation. Geophys. Res. Lett. 34 (17), 1–6. https://doi.org/10.1029/2007GL031166.
Sanz Rodrigo, J., Buchlin, J.M., van Beeck, J., Lenaerts, J.T.M., van den Broeke, M.R., 2013. Evaluation of the antarctic surface wind climate from ERA reanalyses and RACMO2/ANT simulations based on automatic weather stations. Clim. Dyn. 40 (1–2), 353–376. https://doi.org/10.1007/s00382-012-1396-y.
Schmidt, C., Morrison, A.K., England, M.H., 2023. Wind– and Sea-Ice–Driven Interannual Variability of Antarctic Bottom Water Formation. J. Geophys. Res. Oceans 128 (6). https://doi.org/10.1029/2023JC019774.
Schwerdtfeger, W., 1975. The effect of the Antarctic Peninsula on the temperature regime of the Weddell Sea. Mon. Weather Rev. 103 (1), 45–51. https://doi.org/10.1175/1520- 827 0493(1975)1032.0.co;2.
Shen, C., Zha, J., Wu, J., Zhao, D., Azorin-Molina, C., Fan, W., Yu, Y., 2022. Does CRA-40 outperform other reanalysis products in evaluating near-surface wind speed changes over China? Atmos. Res. 266 https://doi.org/10.1016/j.atmosres.2021.105948.
Siegel, S., Castellan Jr., N.J., 1988. Nonparametric Statistics for the Behavioral Sciences, 2nd ed. McGraw-Hill, New York. https://doi.org/10.1177/014662168901300212.
Silvestri, G., Vera, C., 2009. Nonstationary impacts of the southern annular mode on Southern Hemisphere climate. J. Clim. 22 (22), 6142–6148. https://doi.org/10.1175/2009JCLI3036.1.
Tardif, R., Hakim, G.J., Bumbaco, K.A., Lazzara, M.A., Manning, K.W., Mikolajczyk, D.E., Powers, J.G., 2022. Assessing observation network design predictions for monitoring Antarctic surface temperature. Q. J. R. Meteorol. Soc. 148 (743), 727–746. https://doi.org/10.1002/qj.4226.
Tetzner, D., Thomas, E., Allen, C., 2019. A validation of ERA5 reanalysis data in the southern antarctic peninsula—Ellsworth land region, and its implications for ice core studies. Geosciences (Switzerland) 9 (7). https://doi.org/10.3390/geosciences9070289.
Thompson, D.W.J., Solomon, S., 2002. Interpretation of recent Southern Hemisphere climate change. Science 296 (5569), 895–899. https://doi.org/10.1126/science.1069270.
Torralba, V., Doblas-Reyes, F.J., Gonzalez-Reviriego, N., 2017. Uncertainty in recent near-surface wind speed trends: a global reanalysis intercomparison. Environ. Res. Lett. 12 (11) https://doi.org/10.1088/1748-9326/aa8a58.
Turner, J., Colwell, S.R., Marshall, G.J., Lachlan-Cope, T.A., Carleton, A.M., Jones, P.D., Lagun, V., Reid, P.A., Iagovkina, S., 2004. The SCAR READER project: toward a high-quality database of mean Antarctic meteorological observations. J. Clim. 17 (14), 2890–2898. https://doi.org/10.1175/1520-0442(2004)017<2890:TSRPTA>2.0.CO;2.
Turner, J., Colwell, S.R., Marshall, G.J., Lachlan-Cope, T.A., Carleton, A.M., Jones, P.D., Lagun, V., Reid, P.A., Iagovkina, S., 2005. Antarctic climate change during the last 50 years. Int. J. Climatol. 25 (3), 279–294. https://doi.org/10.1002/joc.1130.
Utrabo-Carazo, E., Azorin-Molina, C., Serrano, E., Aguilar, E., Brunet, M., Guijarro, J.A., 2022. Wind stilling ceased in the Iberian Peninsula since the 2000s. Atmos. Res. 272 https://doi.org/10.1016/j.atmosres.2022.106153.
Van Wessem, J.M., Reijmer, C.H., Van De Berg, W.J., Van Den Broeke, M.R., Cook, A.J., Van Ulft, L.H., Van Meijgaard, E., 2015. Temperature and wind climate of the Antarctic Peninsula as simulated by a high-resolution Regional Atmospheric climate Model. J. Clim. 28 (18), 7306–7326. https://doi.org/10.1175/JCLI-D-15-0060.1.
Vautard, R., Cattiaux, J., Yiou, P., Thépaut, J.N., Ciais, P., 2010. Northern Hemisphere atmospheric stilling partly attributed to an increase in surface roughness. Nat. Geosci. 3 (11), 756–761. https://doi.org/10.1038/ngeo979.
Wang, Y., Ding, M., Reijmer, C.H., Smeets, P.C.J.P., Hou, S., Xiao, C., 2021. The AntSMB dataset: a comprehensive compilation of surface mass balance field observations over the Antarctic Ice Sheet. Earth Syst. Sci. Data 13 (6), 3057–3074. https://doi.org/10.5194/essd-13-3057-2021.
Wang, Y., Zhang, X., Ning, W., Lazzara, M.A., Ding, M., Reijmer, C.H., Smeets, P.C.J.P., Grigioni, P., Heil, P., Thomas, E.R., Mikolajczyk, D., Welhouse, L.J., Keller, L.M., Zhai, Z., Sun, Y., Hou, S., 2023. The AntAWS dataset: a compilation of Antarctic automatic weather station observations. Earth Syst. Sci. Data 15 (1), 411–429. https://doi.org/10.5194/essd-15-411-2023.
Wever, N., 2012. Quantifying trends in surface roughness and the effect on surface wind speed observations. J. Geophys. Res. Atmos. 117 (11) https://doi.org/10.1029/2011JD017118.
Wieringa, J., 1989. Shapes of annual frequency distributions of wind speed observed on high meteorological masts.
Wohland, J., Omrani, N.E., Witthaut, D., Keenlyside, N.S., 2019. Inconsistent wind speed trends in current twentieth century reanalyses. J. Geophys. Res. Atmos. 124 (4), 1931–1940. https://doi.org/10.1029/2018JD030083.
Xu, M., Yu, L., Liang, K., Vihma, T., Bozkurt, D., Hu, X., Yang, Q., 2021. Dominant role of vertical air flows in the unprecedented warming on the Antarctic Peninsula in February 2020. Commun. Earth Environ. 2 (1), 1–9. https://doi.org/10.1038/s43247-021-00203-w.
Yu, L., Zhong, S., 2019a. Strong wind speed events over Antarctica and its surrounding oceans. J. Clim. 32 (12), 3451–3470. https://doi.org/10.1175/JCLI-D-18-0831.1.
Yu, L., Zhong, S., 2019b. The interannual variability of surface winds in Antarctica and the Surrounding Oceans: a climatological analysis using the ERA-interim reanalysis data. J. Geophys. Res. Atmos. 124 (16), 9046–9061. https://doi.org/10.1029/2019JD030328.
Yu, L., Zhong, S., Sun, B., 2020. The climatology and trend of surface wind speed over Antarctica and the Southern Ocean and the implication to wind energy application. Atmosphere 11 (1), 108. https://doi.org/10.3390/atmos11010108.
Zapponini, M., Goessling, H.F., 2024. Atmospheric destabilization leads to Arctic Ocean winter surface wind intensification. Commun. Earth Environ. 5 (1) https://doi.org/10.1038/s43247-024-01428-1.
Zeng, Z., Ziegler, A.D., Searchinger, T., Yang, L., Chen, A., Ju, K., Piao, S., Li, L.Z.X., Ciais, P., Chen, D., Liu, J., Azorin-Molina, C., Chappell, A., Medvigy, D., Wood, E.F., 2019. A reversal in global terrestrial stilling and its implications for wind energy production. Nat. Clim. Chang. 9 (12), 979–985. https://doi.org/10.1038/s41558-019-0622-6.
Zhang, Z., Wang, K., 2020. Stilling and recovery of the surface wind speed based on observation, reanalysis, and geostrophic wind theory over China from 1960 to 2017. J. Clim. 33 (10), 3989–4008. https://doi.org/10.1175/JCLI-D-19-0281.1.
Zhang, G., Azorin-Molina, C., Chen, D., Guijarro, J.A., Kong, F., Minola, L., McVicar, T. R., Son, S.W., Shi, P., 2020. Variability of daily maximum wind speed across China, 1975-2016: an examination of likely causes. J. Clim. 33 (7), 2793–2816. https://doi.org/10.1175/JCLI-D-19-0603.1.